

Adaptive plasticity in the spinal cord can produce reaching from scratch and reproduces motor cortex directional tuning

Sergio Verduzco-Flores^{1,2} and Erik De Schutter¹

¹Computational Neuroscience Unit, OIST

²Neural Computation Unit, OIST

Abstract

How dynamic interactions between nervous system regions in mammals performs online motor control remains an unsolved problem. Here we present a new approach using a minimal model comprising spinal cord, sensory and motor cortex, coupled by long connections that are plastic. It succeeds in learning how to perform reaching movements of a planar arm with 6 muscles in several directions from scratch. The model satisfies biological plausibility constraints, like neural implementation, transmission delays, local synaptic learning and continuous online learning. The model can go from motor babbling to reaching arbitrary targets in less than 10 minutes of *in silico* time. Movements are ataxic, as in a motor system without a cerebellum. As emergent properties, neural populations in motor cortex show directional tuning and oscillatory dynamics, and the spinal cord creates convergent force fields that add linearly. The model is extensible and may eventually lead to complete motor control simulation.

1 Introduction

1.1 The challenge

Neuroscience has made great progress in decoding how cortical regions perform specific brain functions like primate vision [1, 2] and rodent navigation [3, 4]. Conversely, the evolutionary much older motor control system still poses fundamental questions, despite a large body of experimental work. This is because, in mammals, in addition to areas in cortex like premotor and motor areas and to some degree sensory and parietal ones, many *extracortical regions* have important and unique functions: basal ganglia, thalamus, cerebellum, pons, brain stem nuclei like the red nucleus and spinal cord [5, 6]. These structures are highly interconnected by fast conducting axons and all show strong dynamic activity changes, related to the ongoing dynamics of the performed motor act.

Clinical and lesion studies have confirmed the necessity of each of these regions for normal smooth motor control of arm reaching [7, 8].

Fully understanding motor control will thus entail understanding the simultaneous function and interplay of all brain regions involved. Little by little, new experimental techniques will allow us to monitor more neurons, in more regions, and for longer periods [9, e.g.]. But to make sense of these data computational models must step up to the task of integrating all those regions to create a functional neuronal machine.

Finally, relatively little is known about the neural basis of motor development *in infants* [10]. Nevertheless, a full understanding of primate motor control will not only require explanation of how these brain regions complement and interact with each other but also how this can be learned during childhood.

With these challenges in mind we recently developed a motor control framework based on differential Hebbian learning [11]. A common theme in physiology is the control of *homeostatic variables* (e.g. blood glucose levels, body temperature, etc.) using negative feedback mechanisms [12]. From a broad perspective, our approach considers the musculoskeletal system as an extension of this homeostatic control system: movement aims to make the external environment conducive to the internal control of homeostatic variables (e.g. by finding food, or shelter from the sun).

Since the muscle contractions do not directly affect the homeostatic variables, how do we make useful movements? This remains unknown, but the best strategy seems to involve various types of learning [13], and hierarchical control [14]. The limbic system provides a link to the levels of homeostatic variables, and has an innate knowledge of rewards and aversions for the organism, so it sits atop the control hierarchy. Down at the bottom, the motor cortex sends signals to the spinal cord, and other areas, to correct errors in the desired value of higher-level variables. This paper explains how the flexible error-reduction mechanism in [11] can explain the interplay between cortex and spinal cord.

1.2 Relevant findings in motor control

Before describing our modeling approach, we summarize some of the relevant experimental data that will be important to understanding the results. We focus on three related issues: 1) the role of the spinal cord in movement, 2) the nature of representations in motor cortex, and 3) muscle synergies, and how the right pattern of muscle activity is produced.

For animals to move, spinal motoneurons must activate the skeletal muscles. In general, descending signals from the corticospinal tract do not activate the motoneurons directly, but instead provide input to a network of excitatory and inhibitory interneurons [15, 16, 17, 18, 19, 20, 21, 22]. Learning even simple behaviors involves long-term plasticity, both at the spinal cord (SC) circuit, and at higher regions of the motor hierarchy [23, 24, 25, 26, 27]. Despite its obvious importance, there are comparatively few attempts to elucidate the nature of the SC computations, and the role of synaptic plasticity.

The role ascribed to SC is closely related to the role assumed from motor cortex, particularly M1. One classic result is that M1 pyramidal neurons of macaques activate preferentially when the hand is moving in a particular direction. When the preferred directions of a large population of neurons are added as vectors, a population vector appears, which points close to the hand's direction of motion [28, 29]. This launched the hypothesis that M1 represents kinematic, or other high-level parameters of the movement, which are transformed into movements in concert with the SC. This hypothesis mainly competes with the view that M1 represents muscle forces. Much research has been devoted to this issue [30, 31, 32, 33, 34, 35, 36, 37, e.g.].

Another important observation is that the preferred directions of motor neurons cluster around one main axis. As shown in [38], this suggests that M1 is mainly concerned with dynamical aspects of the movement, rather than representing its kinematics.

A related observation is that the preferred directions in M1 neurons experience random drifts that overlap learned changes [39, 40]. This leads to the hypothesis that M1 is a redundant network that is constantly using feedback error signals to capture the *task-relevant dimensions*, placing the configuration of synaptic weights in an *optimal manifold*.

A different perspective for studying motor cortex is to focus on how it can produce movements, rather than describing its activity [41]. One specific proposal is that motor cortex has a collection of pattern generators, and specific movements can be created by combining their activity [41, 42]. Experimental support for this hypothesis came through the surprising finding of rotational dynamics in motor cortex activity [43], suggesting that oscillators with different frequencies are used to produce desired patterns. This begs the question of how the animal chooses its desired patterns of motion.

Selecting a given pattern of muscle activation requires *planning*. Motor units are the final actuators in the motor system, but they number in the tens of thousands, so planning movements in this space is unfeasible. A low-dimensional representation of desired limb configurations (such as the location of the hand in Euclidean coordinates) is better. Movement generation likely involves a coordinate transformation, from the endpoint coordinates (e.g. hand coordinates) into actuator coordinates (e.g. muscle lengths), from which motor unit activation follows directly. Even using pure engineering methods, as for robot control, computing this coordinate transformation is very challenging. For example, this must overcome kinematic redundancies, as when many configurations of muscle lengths put the hand in the same location.

The issue of coordinate transformation is central for motor control [7, 44, 45]; *motor primitives and muscle synergies* are key concepts in this discussion. Representing things as combinations of elementary components is a fundamental theme in applied mathematics. For example, linear combinations of basis vectors can represent any vector, and linear combinations of wavelets can approximate any smooth function [46]. In motor control, this idea arises in the form of motor primitives. Motor primitives constitute a set of basic motions, such that that any movement can be decomposed into them [47, 48, 49]. This is closely related to

the concept of synergies. The term “synergy” may mean several things [50, 51], but in this paper we use it to denote a pattern of muscle activity arising as a coherent unit. Synergies may be composed of motor primitives, or they may be the motor primitives themselves.

A promising candidate for motor primitives comes in the form of convergent force fields [52, 53]. In experiments where the limb of a frog or a rat is held at a particular location, local stimulation of the spinal cord will cause a force to the limb’s endpoint. The collection of these force vectors for all of the limb endpoint’s positions forms a force field, and these force fields have two important characteristics: 1) they have a unique fixed point, and 2) simultaneous stimulation of two spinal cord locations produces a force field which is the sum of the force fields from stimulating the two locations independently. It is argued that movement planning may be done in terms of force fields, since they can produce movements that are resistant to perturbations, and also permit a solution to the problem of coordinate transformation with redundant actuators [48].

The neural origin of synergies, and whether they are used by the motor system is a matter of ongoing debate [54, 55, 56]. To us, it is of interest that single spinal units (termed Motor Synergy Encoders, or MSEs) can reliably produce specific patterns of motoneuron activation [57].

1.3 Model concepts

We believe that it is impossible to understand the complex dynamical system in biological motor control without the help of computational modeling. Therefore we set out to build a minimal model that could eventually control an autonomous agent, while still satisfying biological plausibility constraints.

Design principles and biological-plausibility constraints for neural network modeling have been proposed before [58, 59, 60]. Placing emphasis on the motor system, we compiled a set of characteristics that cover the majority of these constraints. Namely:

- **Spanning the whole sensorimotor loop.**
- **Using only neural elements. Learning their connection strengths is part of the model.**
- **Learning does not rely on a training dataset. It is instead done by synaptic elements using local information.**
- **Learning arises from continuous-time interaction with a continuous-space environment.**
- **There is a clear vision on how the model integrates with the rest of the brain in order to enact more general behavior.**

Our aim is hierarchical control of homeostatic variables, with the spinal cord and motor cortex at the bottom of this hierarchy. At first glance, spinal plasticity poses a conundrum, because it changes the effect of corticospinal inputs.

Cortex is playing a piano that keeps changing its tuning. A solution comes when we consider the corticospinal loop (e.g. the long-loop reflex) as a negative control system, where the spinal cord activates the effectors to reduce an error. The role of cortex is to produce perceptual variables that are controllable, and can eventually improve homeostatic regulation. In this regard, our model is a variation of Perceptual Control Theory [61, 62], but if the desired value of the controller is viewed as a prediction, then this approach resembles active inference models [63].

Quite importantly, the motor cortex does not send a command but an error, so it is a potential learning signal for the spinal circuits involving interneurons and their afferent inputs. In this way, the spinal circuit could learn to produce simple motor programs on its own, guided by descending signals [27, 64, 65].

All this can work only when the spinal cord can find the input-output structure of the feedback controller implicit in the long-loop reflex. In other words, finding which motoneurons are effective for reducing a given error signal. We have found that this important problem can be solved in a biologically-plausible manner by using the correlations between the derivatives of two activities: those of corticospinal axons, and those of spinal interneurons. The learning rules that make this possible were introduced in [11], where it was also shown how they could be combined with reinforcement learning to handle cases where correlations depend on the external context. But [11] did not illustrate biologically realistic examples, and did not clearly show the viability of its learning rules as a plasticity mechanism in the spinal cord. We fill those gaps in this paper, using a model that satisfies the characteristics outlined above. Furthermore, we show that many phenomena described in section 1.2 emerge from this system.

2 Results

2.1 A neural architecture for motor control

The model in this paper contains the main elements of the long-loop reflex, applied to the control of a planar arm using six muscles. The left panel of figure 1 shows the architecture of the model, which contains 74 firing rate neurons organized in six populations. This architecture resembles a feedback controller that makes the activity in a neural population S_A approach the activity in a different population S_P .

The six firing-rate neurons (called *units* in this paper) in S_A represent a region of somatosensory cortex, and its inputs consist of the static gamma (II) afferents. In steady state, activity of the II afferents is monotonically related to muscle length [66], which in turn can be used to prescribe hand location.

S_P represents a different cortical layer of the same somatosensory region as S_A , where a “desired” or “predicted” activity has been caused by brain regions not represented in the model. Each firing rate neuron in S_A has a corresponding unit in S_P , and they represent the mean activity at different levels of the same microcolumn [67]. S_{PA} is a region that conveys the difference between activities

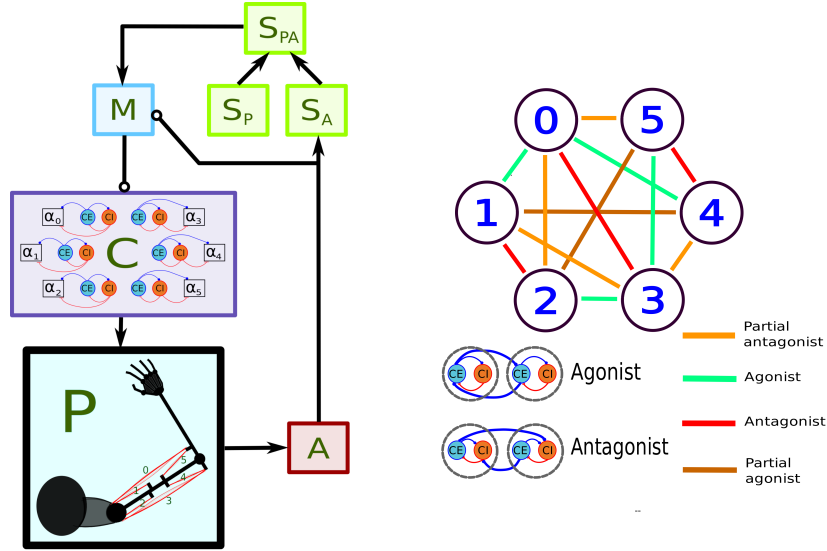


Figure 1: Main components of the model. In the left panel each box stands for a neural population, except for **P**, which represents the arm and the muscles. Arrows indicate the direction of connectivity. Connections with an open circle indicate plastic synapses. **A**: afferent population. **S_A**: Somatosensory cortex, modulated by afferent input. **S_P**: somatosensory cortex, prescribed pattern. **S_{PA}**: population signaling the difference between **S_P** and **S_A**. **M**: primary motor cortex. **C**: spinal cord. Inside the **C** box the circles represent the excitatory (**CE**) and inhibitory (**CI**) interneurons, organized into six pairs. The interneurons in each pair innervate an alpha motoneuron (α), each of which stimulates one of the six muscles in the arm, numbered from 0 to 5. The trios consisting of **CE**, **CI**, α units are organized into agonists and antagonists, depending on whether their α motoneurons cause torques in similar or opposite directions. These relations are shown in the right-side panel.

in S_P and S_A , which is the error signal minimized by negative feedback control.

Population A represents sensory thalamus and dorsal parts of the spinal cord. It contains 18 units with logarithmic activation functions, each receiving an input from a muscle afferent. Each muscle provides proprioceptive feedback from models of the Ia, Ib, and II afferents. In rough terms, Ia afferents provide information about contraction velocity, and Ib afferents signal the amount of tension in the muscle and tendons.

The population M represents motor cortex. One input to M is a static linear combination of the S_{PA} errors. This is combined with afferent Ia, Ib inputs arising from population A . Synapses from A use a variation of the *input correlation* learning rule [68], where the S_{PA} input acts as a learning signal. This learning rule enhances the stability of the controller. More details are presented in Methods.

To represent excitatory and inhibitory neuron populations, both M and S_{PA} use a “dual representation”, where each error signal is represented by two units. Let $e_i = s_P^i - s_A^i$ be the error associated with the i -th muscle. One of the two S_{PA} units representing e_i is a monotonic function of $\max(e_i, 0)$, whereas the other unit increases according to $\max(-e_i, 0)$. These opposing inputs, along with mutual inhibition between the two units creates dynamics where sensorimotor events cause both excitatory and inhibitory responses, which agrees with experimental observations [69, 70, 71], and allows transmitting “negative” values. Dual units in M receive the same inputs, but with the opposite sign.

The task of specifying which muscles should be activated in order to reduce S_{PA} errors is performed by a “spinal” network C that transforms the M outputs into muscle stimulation. C learns to transform sensory errors into appropriate motor commands using a differential Hebbian learning rule [11].

To explain the idea behind this rule, assume that C contains N interneurons, whose activity vector we denote as $\mathbf{c} = [c_1, \dots, c_N]$. The input to each of these units is an M -dimensional vector $\mathbf{e} = [e_1, \dots, e_M]$. Each unit in C has an output $c_i = \sigma\left(\sum_j \omega_{ij} e_j\right)$, where $\sigma(\cdot)$ is a positive sigmoidal function. The inputs are assumed to be errors, and to reduce them we want e_j to activate c_i when c_i can reduce e_j . One way this could happen is when the weight ω_{ij} from e_j to c_i is proportional to the negative of their sensitivity derivative:

$$\omega_{ij} \propto -\frac{\partial e_j}{\partial c_i}. \quad (1)$$

Assuming a monotonic relation between the motor commands and the errors, relation 1 entails that errors will trigger an action to cancel them, with some caveats considered in [11]. Synaptic weights akin to equation 1 can be obtained using a learning rule that extracts correlations between the derivatives of c_i and e_j (see Methods). Using this rule, the commands coming from population C can eventually move the arm so that S_A activity resembles S_P activity.

C is organized to capture the most basic motifs of spinal cord connectivity using a network where balance between excitation and inhibition is crucial [72, 73]. Each one of six α motoneurons stimulate one muscle, and is stimulated by one excitatory (CE), and one inhibitory (CI) interneuron. CE and CI stimulate one another, resembling the classic Wilson-Cowan model [74]. The trios composed of α , CE , and CI neurons compose a group that controls the activation of one muscle, with CE and CI receiving convergent inputs from M . (α , CE , CI) trios are connected to other trios following the agonist-antagonist motif that is common in the spinal cord [75]. This means that CE units project to the CE units of agonists, and to the CI units of antagonists (figure 1, right panel). When the agonist/antagonist relation is not strongly defined, muscles can be “partial” agonists/antagonists, or unrelated.

Because timing is essential to support the conclusions of this paper, every connection has a transmission delay, and all firing rate neurons are modeled with ordinary differential equations. Direct connections from A to C (the “short-loop reflex”) are not included in this model (See Supplemental information, section

6.3).

2.2 The model can reach by matching perceived and desired sensory activity

Reaches are performed by specifying an S_P pattern equal to the S_A activity when the hand is at the target. The acquisition of these S_P patterns is not in the scope of this paper (but see [11]).

We created a set of random targets by sampling uniformly from the space of joint angles. Using this to set a different pattern in S_P every 40 seconds, we allowed the arm to move freely. To produce exploratory movements we used noise in the CE , CI units, plus two additional units described in the Methods (4.3), called ACT , and CHG . ACT is a leaky integrator of the total activity in S_{PA} , reflecting the total error, and triggers adaptation in CE and CI when a threshold is crossed. CHG is connected to ACT in order to reset its activity when a new target is presented.

For a typical set of random initial weights, the system was capable of reaching roughly after 5 different targets were presented, which can be seen in figure 2A. This figure shows the error (the distance between the hand and the target) through 16 successive reaches (640 seconds of *in-silico* time). The 16 reaches of this training phase can also be observed in the supplementary video SV1. In figure 2A the error suddenly increased each time a new target was presented (yellow vertical lines), but as learning continued this error was consistently reduced below 10 centimeters before the next target was presented.

Statistics concerning how different initial synaptic weights affect this error are presented in supplemental section 10.

Panel B also shows the effect of learning, as the hand’s Cartesian coordinates eventually track the target coordinates whenever they change. This is also reflected as the activity in S_A becoming similar to the activity in S_P (panel C).

Panels D and E of figure 2 show the activity of a few units in populations M and C during the 640 seconds of this training phase. During the first few reaches, M shows a large imbalance between the activity of units and their duals, reflecting larger errors. Eventually these activities balance out, leading to mild, homogeneous activity that may spike when a new target appears. M1 activation patterns that produce no movement are called the *null-space activity* [76]. In our case, this includes patterns where M units have the same activity as their duals.

In panel E the noise in the C units becomes evident. It can also be seen that inhibition dominates excitation (due to CE to CI connections), which promotes stability in the circuit.

We tested whether any of the novel elements in the model were superfluous. To this end, we removed each of the elements individually and checked if the model could still learn to reach (see Supplemental information, section 11).

As expected, removing the plasticity in the connections from M to C destroyed any resemblance of reaching when starting from random connectivity (figures S13A,B; S14A). Removing the plasticity in the connections from A to M

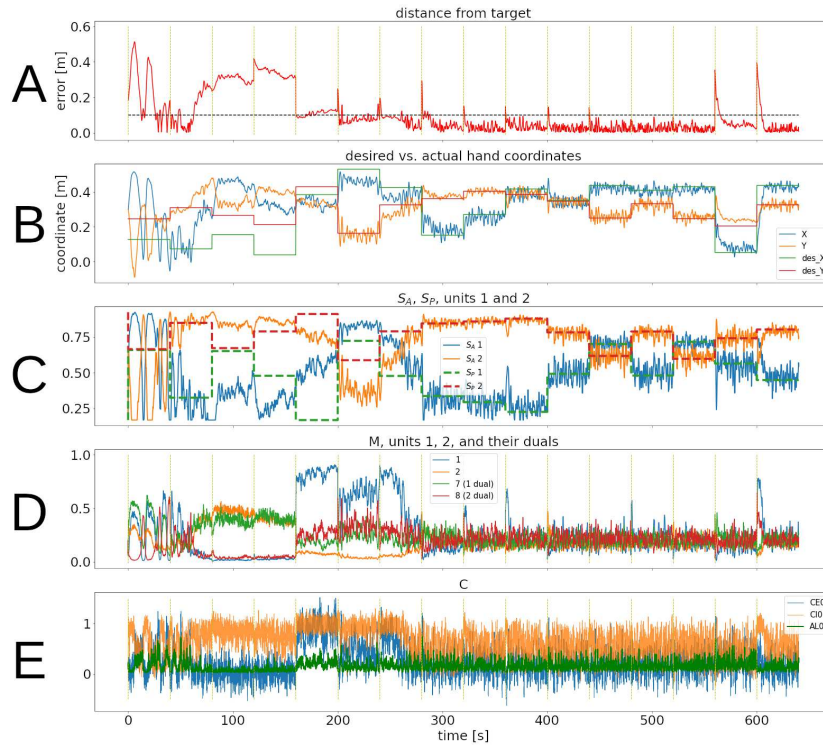


Figure 2: Training phase of the simulation. **A:** Distance between the target and the hand through 640 seconds of simulation, corresponding to 16 reaches to different targets. The dotted line corresponds to 10 centimeters. The times when S_P changes are indicated with a vertical, dotted yellow line. **B:** Desired versus actual hand coordinates through the training phase. **C:** Activity of units 1 and 2 in S_P and S_A . **D:** Activity of M units 1, 2, and their duals. **E:** Activity of the CE, CI, α trio for muscle 0.

resulted in oscillations too extreme to allow reaching (figures S13C,D; S14B). This seems consistent with the effects of deafferentation, which destroys the stability of movements when combined with cerebellar damage [77].

We attempted to remove the Ia and Ib afferents from the model, sending the II afferent signal to both M and S_A . We failed to make this network reach (figures S13D,E; S14C).

Removing the agonist-antagonist connections in C increased the time required to learn by almost an order of magnitude, and in some cases increased the endpoint error, but it was still possible to reach in the absence of these connections.

Removing the ACT unit disabled learning for most initial conditions tested. The same thing happened when noise was removed from the units in C .

2.3 Spinal interneurons can also activate combinations of motoneurons

As shown above, there is a one-to-one relation between the α motoneurons and pairs of CE, CI units. However, there is evidence for interneurons that drive a set of muscles, possibly setting the circuit foundation for motor synergies [47, 56, 57]. We thus explored whether reaching can be learned when the CE and CI units send projections to more than one motoneuron.

We modified the architecture of figure 1 so that for every combination of two different muscles there were CE, CI units that stimulated both of them (see Methods).

We found that all the results in this paper also hold for this “synergistic” configuration. More details are in the Supplementary information, section 7.

2.4 Center-out reaching 1: The reach trajectories present traits of cerebellar ataxia

In order to compare our model with experimental data, after the training phase we began a standard center-out reaching task. Switching the task merely consisted of presenting the targets in a different way, but for the sake of smoother trajectories we removed the noise from the units in C . The noise in C does not impair reaching, but it causes random variations in the hand’s trajectory (Supplementary information, section 9).

Figure 3A shows the 8 peripheral targets around a hand rest position. Before reaching a peripheral target, a reach to the center target was performed, so the whole experiment was a single continuous simulation.

Peripheral targets were selected at random, each appearing 6 times. This produced 48 reaches (without counting reaches to the center), each one lasting 5 seconds. Supplementary section 8 shows the activity of selected units during this period, along with the evolution of several synaptic weights. Panels B and C of figure 3 show the trajectories followed by the hand in two scenarios.

The most straightforward way to connect S_{PA} and M is to use one-to-one connectivity, where each M unit controls the length error of one muscle.

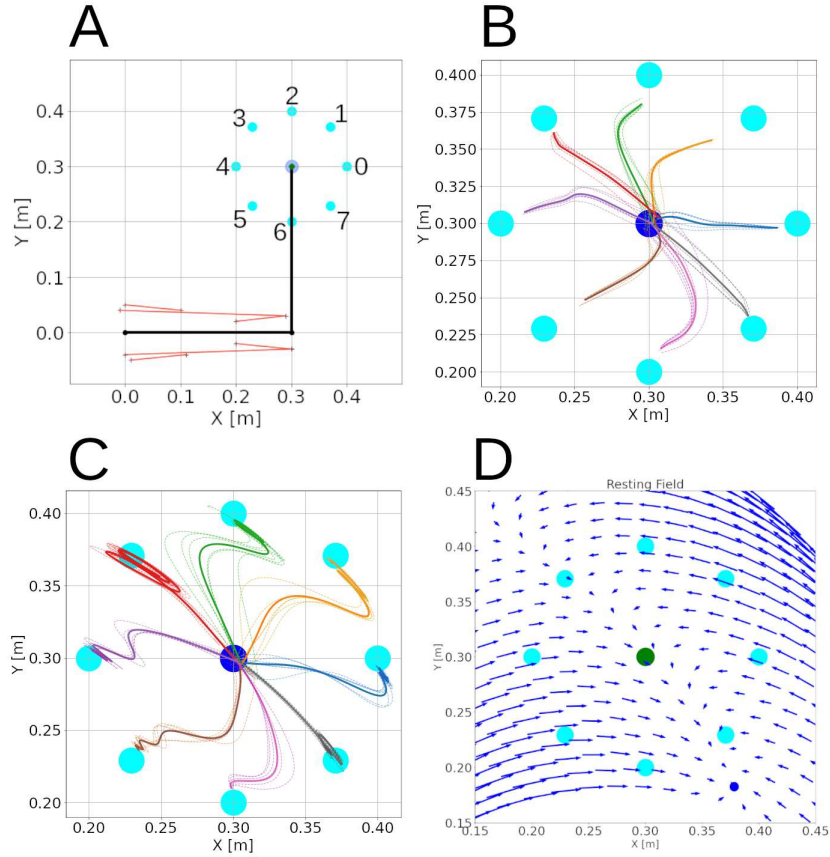


Figure 3: Center-out reaching. **A**: The arm at its resting position, with hand coordinates (0.3, 0.3), where a center target is located. Eight peripheral targets (cyan dots) were located on a circle around the center target, with a 10 cm radius. The muscle lines, connecting the muscle insertion points, are shown in red. The shoulder is at the origin, whereas the elbow has coordinates (0.3, 0). Shoulder insertion points remain fixed. **B**: Hand trajectories for all reaches using one-to-one connectivity between S_{PA} and M . Thick lines are the average of the 6 reaches (dotted lines) to each target. **C**: Hand trajectories when using a linear combination of errors for each M unit. **D**: The resting direction field (defined in section 2.8) and the targets. Arrows show where the hand goes in 0.5 seconds when it starts from rest at the base of the arrow. No inputs are applied to the spinal cord, but its intrinsic activity still stimulates the muscles, shifting the fixed point (blue dot).

Interestingly, this does not lead to the best performance, as shown in figure 3B. Instead, it is better to have each unit in M be driven by a linear combination of S_{PA} errors (figure 3C). Not all connection matrices between S_{PA} and M lead to the same performance, and this has not been systematically explored (see Methods, section 4.9.) Still, the fact that a mix of errors can be used to control reaching even when spinal interneurons stimulate several motoneurons (supplementary sections 7, 10) offers a new perspective on how control could arise in the face of convergent and redundant sensorimotor loops [78].

Currently our system has neither cerebellum nor visual information. Lacking a “healthy” model to make quantitative comparisons, we analyzed qualitative properties of the trajectories.

For the sake of stability and simplicity, our system is configured to perform slow movements. Fast and slow reaches are different in cerebellar patients [79]. Slow reaches undershoot the target, follow longer hand paths, and show movement decomposition (joints appear to move one at a time). This is consistent with figure 3B,C, as well as with figure 4.

The shape of the trajectory depends largely on the target. Different reach directions cause different interaction forces, and encounter different levels of viscoelastic resistance from the muscles. In figure 3D the arrows approximate the magnitude and direction of this resistance for different locations of the hand.

Figure 4 reveals that the approach to the target is initially fast, but gradually slows down. Healthy subjects usually present a bell-shaped velocity profile, with some symmetry between acceleration and deceleration. This symmetry is lost with cerebellar ataxia [77, 80].

We are not aware of center-out reaching studies for cerebellar patients in the dark, but [81] does examine reaching in these conditions. Summarizing its findings:

1. Movements were slow.
2. The endpoints had small variation, but they had constant errors.
3. Longer, more circuitous trajectories, with most changes in direction during the last quarter.
4. Trajectories to the same target showed variations.

These seem consistent with panel C of figure 3 for several reach directions, but the last 2 traits may not apply to panel B with the less plausible one-to-one connections. The traits are more evident in versions of the model using synergistic connections, and when the noise is not removed (see Supplementary information, sections 7, 9).

2.5 Center-out reaching 2: Directional tuning and preferred directions

To find whether directional tuning could arise during learning, we analyzed the M population activity for the 48 radial reaches described in the previous

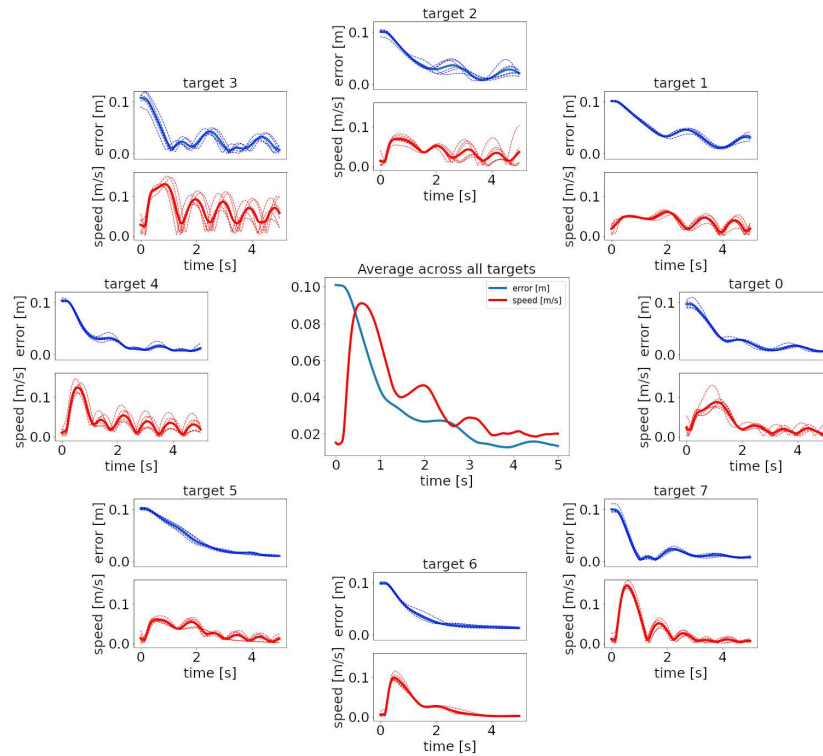


Figure 4: Distance to target and reach velocity through time for the 8 individual targets. The center plot shows the average distance to target (blue line) and the hand velocity (red line) through five seconds of the reach. The peripheral plots show the error (blue line, top) and velocity (red line, bottom) when reaching to individual targets, numbered as in figure 3A. The thick continuous traces are the average over six reaches. Dotted lines show individual trajectories.

subsection.

For each of the 12 units in M , figure 5A shows the mean firing rate of the unit when reaching each of the 8 targets. The red arrows show the Preferred Direction (PD) vectors that arise from these distributions of firing rates. For the sake of the next exposition, figure 5 shows data for the simpler case of one-to-one connectivity between S_{PA} and M , but these results generalize.

We found that 10 units were significantly tuned to reach direction ($p < 0.001$, bootstrap test), with PD vectors of various lengths. The direction of the PD vectors is not mysterious. Each M unit controls the length error of one muscle (assuming one-to-one S_{PA} to M connections). Figure 5B shows that the required contraction length depends on both the target and the muscle. The PD vectors of units 0-5 point to the targets that require the most contraction of their muscle. Units 6-11 are the duals of 0-5, and their PD is in the opposite direction. Figure 5C shows that the PD may also be inferred from the muscle activity, reflected as average tension. The pattern of wedges in corresponding plots of panels A and C may or may not be alike, which means that correlations between firing rates and muscle activity will vary.

In the case when each M unit receives a linear combination of S_{PA} errors, its PD can be predicted using a linear combination of the “directions of maximum contraction” shown in figure 5B, using the same weights as the S_{PA} inputs. When accounting for the length of the PD vectors, this can predict the PD angle with a coefficient of determination $R^2 \approx 0.96$.

As mentioned in the Introduction, the PDs of motor cortex neurons tend to align in particular directions [38]. This is almost trivially true for this model, since the PD vectors are mainly produced by linear combinations of the vectors in figure 5B.

Figure 6 is a plot containing the PD vectors for all the cells in figure 5. The PD distribution shows significant bimodality ($p < 0.001$), with the PDs concentrated around a line at approximately 61 degrees.

To compare with [38] we rotate this line 45 degrees so the targets are in the same position relative to the shoulder (e.g. [82] Fig. 1, [83] Fig. 1). This places the main axis for the PDs on the 106-286 degree axis, comparable to the 117-297 axis in [38].

The study in [82] suggested that a rudimentary spinal cord feedback system should be used to understand *why* the PD distribution arises. Our model is the first to achieve this prediction.

The PD vectors are not stationary, but experience random fluctuations that become more pronounced in new environments [39, 40]. The brain is constantly remodeling itself, without losing the ability to perform its critical operations [84]. Our model is continuously learning, so we tested the change in the PDs by setting 40 additional center-out reaches (no intrinsic noise) after the previous experiment. To encourage changes we set 10 different targets instead of 8. After the additional reaches the PDs showed an averaged deviation of 27 degrees. The average distance between hand and target during the 40 reaches was 3 cm.

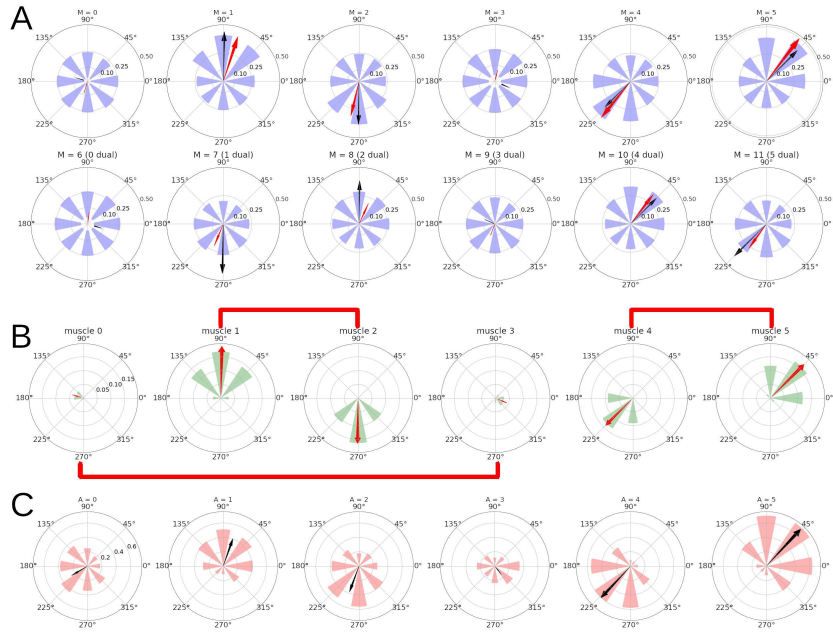


Figure 5: Directional tuning of the units in M . **A**: Average firing rate per target, and preferred direction (see Methods) for each of the 12 units in M . Each polar plot corresponds to a single unit, and each of the 8 purple wedges corresponds to one of the 8 targets. The length of a wedge indicates the mean firing rate when the hand was reaching the corresponding target. The red arrow indicates the direction and relative magnitude of the PD vector. The black arrow shows the predicted PD vector, in this case just the corresponding arrows from panel B. **B**: For each muscle and target, a wedge shows the muscle’s length at rest position minus the length at the target, divided by the rest position length. The red arrow comes from the sum of the wedges taken as vectors, and represents the muscle’s direction of maximum contraction. Plots corresponding to antagonist muscles are connected by red lines. **C**: Average activity of the 6 A units indicating muscle tension. The arrows come from the sum of wedges taken as vectors.

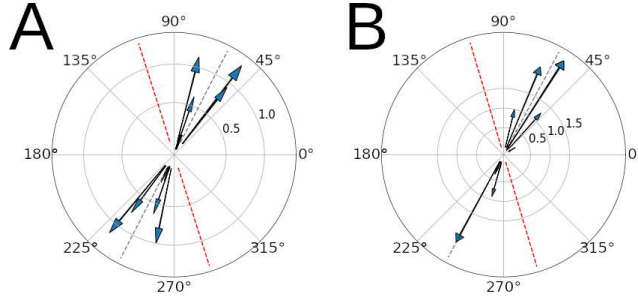


Figure 6: Preferred direction vectors for the 12 M units. The gray dotted line shows the main axis of the distribution. The red dotted line is a 45-degree rotation the gray line, for comparison with [38]. **A**: The case with one-to-one connections between S_{PA} and M . **B**: The case with a non-identity connection matrix between S_{PA} and M .

2.6 Center-out reaching 3: Rotational dynamics

Using a dynamical systems perspective, [41] considers that the muscle activity $\mathbf{m}(t)$ (a vectorial function of time) arises from the cortical activity vector $\mathbf{r}(t)$ after it is transformed by the downstream circuitry:

$$\mathbf{m}(t) = G[\mathbf{r}(t)]. \quad (2)$$

It is considered that the mapping $G[\cdot]$ may consist of sophisticated controllers, but for the sake of simplicity this mapping is considered static, omitting spinal cord plasticity. The cortical activity arises from a dynamical system:

$$\tau \dot{\mathbf{r}}(t) = h(\mathbf{r}(t)) + \mathbf{u}(t), \quad (3)$$

where $\mathbf{u}(t)$ represents inputs to motor cortex from other areas, and $h(\cdot)$ is a function that describes how the state of the system evolves.

A difficulty associated with equation 3 is explaining how $\mathbf{r}(t)$ generates a desired muscle pattern $\mathbf{m}(t)$ when the function $h(\cdot)$ represents the dynamics of a recurrent neural network. One possibility is that M1 has intrinsic oscillators of various frequencies, and they combine their outputs to shape the desired pattern. This prompted the search for oscillatory activity in M1 while macaques performed center-out reaching motions. A brief oscillation (in the order of 200 ms, or 5 Hz) was indeed found in the population activity [43], and the model in [42] was able to reproduce this result, although this was done in the open-loop version of equations 2 and 3, where $\mathbf{u}(t)$ contains no afferent feedback (this is further commented in the Supplemental Discussion, section 6.1).

Recently it was shown that the oscillations in motor cortex can arise when considering the full sensorimotor loop, without the need of recurrent connections in motor cortex [85]. A natural question is whether our model can also reproduce the oscillations in [43] without requiring M1 oscillators or recurrent connections.

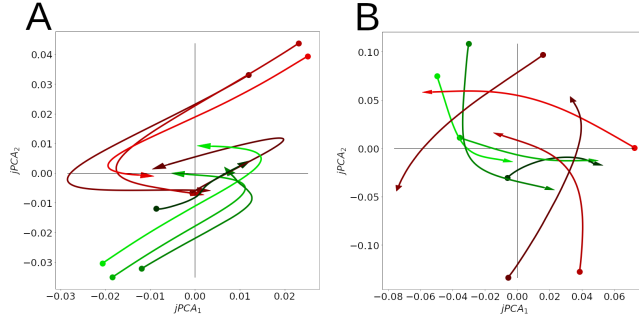


Figure 7: Rotational dynamics in the M population. First two jPCA components during 0.5 seconds, for each of the 8 conditions/targets. Traces are colored according to the magnitude of their initial $jPCA_1$ component, from smallest (green) to largest (red). **A**: One-to-one S_{PA} to M connections. **B**: Non-identity S_{PA} to M connections.

The central part of the analysis in [43] is obtaining the first two jPCA vectors, as they define the plane of strongest rotations. Informally, this means that when the firing rate vector $\mathbf{m}(t)$ of M1 is projected onto this plane, the resulting trajectories show the most rotations.

We replicated the jPCA analysis, with adjustments to account for the smaller number of neurons, the slower dynamics, and the fact that there is no delay period before the reach (See Methods). The result can be observed in figure 7, where 8 trajectories are seen. Each trajectory is the average activity of the 12 M units when reaching to one of the 8 targets, projected onto the jPCA plane. Our model trajectories show the properties from the study in [43]: rotations are prevalent (the first plane out of six captures 50% of the total variance), and the direction of rotation is the same across conditions.

With this analysis we show that the quasi-oscillations observed after reach onset could arise from a sudden increase and subsequent decay of error in the loop. If this is the case, then their decay time should be correlated with the decay time of the error. Notice that this hypothesis is not very different from the interpretation in [86] (Supplemental Discussion, section 6.1), where a rotational movement in state space is observed as velocity rises and then falls.

2.7 Results still hold when the arm changes its mass

Physical properties of the arm can change, not only as the arm grows, but also when tools or new environments come into play. As a quick test of whether the properties in this paper are robust to moderate changes, we repeated the simulations, changing the mass of the arm and forearm from 1 to 0.8 kg.

A lighter arm slightly improved performance, so that the average distance between hand and target during center-out reaching was 3 cm. 9 units were significantly tuned to reaching direction, and the PD vectors could be predicted

with a 0.97 coefficient of determination. The main axis of the PD distribution was at 61.6 degrees (106.6 degrees after a 45 degree rotation), and the first jPCA plane captured 41% of the variance.

In the same simulation, after the center-out reaching was completed, we once more modified the mass of the arm and forearm, from 0.8 to 1.2 kg, after which we began the center-out reaching again.

The heavier arm could still reach normally, with the average distance between hand and target still around 3 cm. PD vectors could be predicted with a 0.94 coefficient of determination. 11 of the units were significantly tuned to direction. The main axis of the PD distribution aligned with 61.7 (106.7) degrees, and the first jPCA plane captured 36% of the variance.

A plot of the hand trajectories of the 0.8 and 1.2 masses can be found in the Supplementary information, section 12.

2.8 Spinal stimulation produces convergent direction fields

Due to the viscoelastic properties of the muscles, the mechanical system without active muscle contraction will have a fixed point with lowest potential energy at the arm’s rest position. Limited amounts of muscle contraction shift the position of that fixed point. This led us to question whether this could produce convergent force fields, which as discussed before are candidate motor primitives, and have been found experimentally.

To simulate local stimulation of an isolated spinal cord we removed all neuronal populations except for those in C , and applied inputs to the individual pairs of CE, CI units projecting to the same motoneuron. Doing this for different starting positions of the hand, and recording its initial direction of motion, produces a *direction field*. A direction field (DF) maps each initial hand location to a vector pointing in the average direction of the force that initially moves the hand.

The first two panels of figure 8 show the result of stimulating individual E-I pairs in C , which will indeed produce DFs with different fixed points.

We found that these DFs add approximately linearly (Fig. 8D). More precisely, let $D(a + b)$ be the DF from stimulating spinal locations a and b simultaneously, and $\alpha_{a+b}(x, y)$ be the angle of $D(a + b)$ at hand coordinates (x, y) . Using similar definitions for $D(a), D(b), \alpha_a(x, y), \alpha_b(x, y)$, we say the DFs add linearly if

$$\alpha_{a+b}(x, y) = \alpha_a(x, y) + \alpha_b(x, y), \quad \forall(x, y).$$

We define the mean angle difference between $D(a + b)$ and $D(a) + D(b)$ as

$$\gamma_{a,b} = \sum_{x,y} \frac{\alpha_{a+b}(x, y) - (\alpha_a(x, y) + \alpha_b(x, y))}{N_s}, \quad (4)$$

where N_s is the number of (x, y) sample points. We found that when averaged over the 15 possible (a, b) pairs, the mean of $\gamma_{a,b}$ was 13.7 degrees.

Randomly choosing two possibly different pairs (a, b) and (c, d) for the stimulation locations leads to a mean angle difference of 33.2 degrees between the

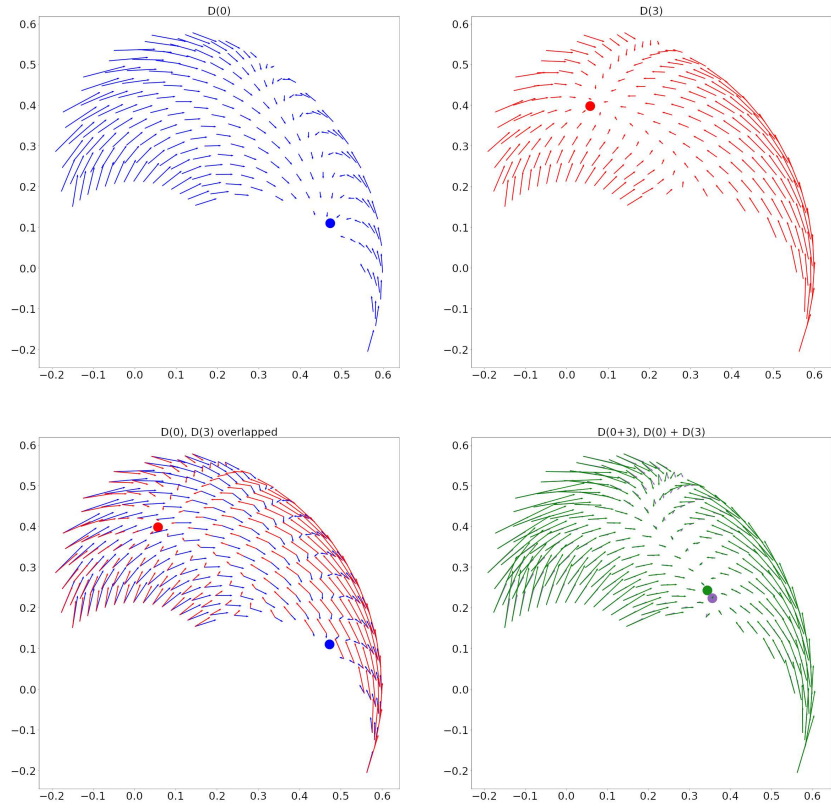


Figure 8: Two sample direction fields and their linear addition. **A:** DF from stimulation of the interneurons for muscle 0 (biarticular biceps). The approximate location of the fixed point is shown with a blue dot. **B:** DF from stimulation of muscle 3 (biarticular triceps) interneurons. A red dot shows the fixed point. **C:** Panels A and B overlapped. **D:** In green, the DF from stimulating the interneurons for muscles 0 and 3 together. In purple, the sum of the DFs from panels A and B. Dots show the fixed points. The average angle between the green and purple vectors is 4 degrees.

fields $D(a + b)$ and $D(c) + D(d)$ fields. A bootstrap test showed that the mean angle difference was significantly smaller when $(a, b) = (c, d)$, ($p < 0.01$).

The resting field is defined as the DF when no units are stimulated (Fig. 3). Removing the resting field from $D(a + b)$, $D(a)$, and $D(b)$ does not alter these results.

3 Discussion

3.1 Summary of findings and predictions

We have presented a model of the long loop reflex with a main assumption: negative feedback configured with differential Hebbian learning rules. One rule sets the input-output structure in the spinal cord, and another produces compound error signals in motor cortex. Emphasis is also placed on the balance between excitation and inhibition. With these elements we produced a model that makes arm reaches by trying to perceive a given afferent pattern.

We list some properties of the model, and possible implications:

- Basic arm reaching happens through negative feedback, trying to perceive a target value set in cortex. Learning the input-output structure of the feedback controller requires spinal cord plasticity.
 - Cerebellar patients should not be able to adapt to tasks that require fast reactions, as negative feedback alone cannot compensate for delays in the system [87]. On the other hand, they should be able to learn tasks that require remapping afferent inputs to movements. One example is [88], where cerebellar patients learned to move in a novel dynamic environment, but their movements were less precise than those of controls.
- Interneurons that stimulate more than one muscle group can be added to the system thanks to the flexibility of the learning rules.
- The shape of reaches is dominated by mechanical and viscoelastic properties of the arm and muscles.
 - Unfamiliar viscous forces as in [88] should predictably alter the trajectory (Fig. 3C) for cerebellar patients, who should not be able to adapt unless they move slowly and are explicitly compensating.
- Preferred Directions (PDs) in motor cortex happen because muscles need to contract more when reaching in certain directions.
 - The PD distribution should align with the directions where the muscles need to contract to reduce the error. These directions depend on which error S_{PA} is encoding. If the error is not related to reaching (e.g. related to haptic feedback), a different PD distribution may arise after overtraining.

- Drift in the PD vectors comes from the ongoing adaptation, and it should not disrupt performance.
- Quasi-oscillations observed in motor cortex activity after the onset of movement reflect the decrease in the error signal.
 - The decay time of quasi-oscillations in motor cortex after movement onset will correlate with the error decay.
- Convergent force fields happen naturally in musculoskeletal systems when there is balance in the stimulation between agonists and antagonists. Linear addition of force fields is a result of forces/torques adding linearly.

Since our relatively simple model could reproduce all these phenomena, we believe it constitutes a good null hypothesis for all of them. But beyond explaining experimental observations, this model makes inroads into the hard problem of how the central nervous system (CNS) can generate effective control signals, recently dubbed the “supraspinal pattern formation” problem [78]. From our perspective, the CNS does not need to generate precise activation patterns for muscles and synergies; it needs to figure out which perceptions need to change. It is subcortical structures that learn the movement details. The key to make such a model work is the differential Hebbian learning framework in [11], which handles the final credit assignment problem.

We choose not to include a model of the cerebellum at this stage. Our model reflects the brain structure of an infant baby who can make clumsy reaching movements. At birth the cerebellum is incomplete and presumably not functional. It requires structured input from spinal cord and cortex to establish correct synaptic connections during postnatal development and will contribute to smooth reaching movements at a later age.

Encompassing function, learning, and experimental phenomena in a single simple model is a promising start towards a more integrated computational neuroscience. Moreover, predictive simple models have the potential to steer complex large-scale models so they can also achieve learning and functionality from scratch.

4 Methods

Simulations were run in the Draculab simulator [89]. All the parameters from the equations in this paper are presented in the Supplementary information (section 14). Parameters not shown can be obtained from Python dictionaries in the source code. This code can be downloaded from:

https://gitlab.com/sergio.verduzco/public_materials/-/tree/master/adaptive_plasticity

4.1 Unit equations

With the exception of the A and S_P populations, the activity u_i of any unit in figure 1 has dynamics:

$$\tau_u \dot{u}_i = \sigma(I) - u_i, \quad (5)$$

$$\sigma(I) = \frac{1}{1 + \exp(\beta(I - \eta))}, \quad (6)$$

where τ is a time constant, β is the slope of the sigmoidal function, η is its threshold, and $I = \sum_j \omega_{ij} u_j(t - \Delta t_j)$ is the sum of delayed inputs times their synaptic weights.

Units in the *CE*, *CI* populations had an additional noise term, which turned equation 5 into this Langevin equation:

$$du_i(t) = \frac{1}{\tau_u} (\sigma(I) - u_i(t)) + \varsigma dW(t), \quad (7)$$

where $W(t)$ is a Wiener process with unit variance, and ς is a parameter to control the noise amplitude. This equation was solved using the Euler-Maruyama method. All other unit equations were integrated using the forward Euler method. The equations for the plant and the muscles were integrated with SciPy's (<https://scipy.org/>) explicit Runge-Kutta 5(4) method.

Units in the *A* population use a rectified logarithm activation function, leading to these dynamics for their activity:

$$\tau_a \dot{a} = \log([1 + I - T]_+) - a, \quad (8)$$

where τ_a is a time constant, I is the scaled sum of inputs, T is a threshold, and $[x]_+ = \max(x, 0)$ is the "positive part" function.

4.2 Learning rules

The learning rule for the connections from *M* to *CE*, *CI* units was first described in [11]. It has an equation:

$$\dot{\omega}_{ij}(t) = -\left(\ddot{e}_j(t) - \langle \ddot{e}(t) \rangle\right) \left(\dot{c}_i(t - \Delta t) - \langle \dot{c}(t - \Delta t) \rangle\right). \quad (9)$$

In this equation, $e_j(t)$ represents the activity of the j -th unit in *M* at time t , and $\ddot{e}_j(t)$ is its second derivative. Angle brackets denote averages, so that $\langle \ddot{e} \rangle \equiv \frac{1}{N_M} \sum_k \ddot{e}_k$, where N_M is the number of *M* units. $\dot{c}_i(t)$ is the derivative of the activity for the postsynaptic unit, and Δt is a time delay ensuring that the rule captures the proper temporal causality.

The learning rule in 9 was also fitted with soft weight-bounding to prevent connections from changing sign, and multiplicative normalization was used to control the magnitude of the weights by ensuring two requirements: (1) all weights from projections of the same *M* unit should add to w_{sa} , (2) all weights ending at the same *C* unit should add to w_{sb} . With this, the learning rule adopted the form:

$$\dot{\omega}_{ij} = -\alpha \omega_{ij} \left(-\Delta + \lambda [(0.5(\zeta_{sa} + \zeta_{sb}) - 1)] \right), \quad (10)$$

In this equation α is a constant learning rate, Δ is the right-hand side expression of equation 9, and λ is a scalar parameter. The value ζ_{sa} is w_{sa} divided by the sum of outgoing weights from the j -th M unit, and ζ_{sb} is w_{sb} divided by the sum of incoming M weights on c_i . This type of normalization is meant to reflect the competition for resources among synapses, both at the presynaptic and postsynaptic level.

The synapses in the connections from A to M used the input correlation rule [68]:

$$\dot{w} = \alpha_{IC} w I_A \dot{I}_{PA}, \quad (11)$$

where I_A is the scaled sum of inputs from the A population, α_{IC} is the learning rate, I_{PA} is the scaled sum of inputs from S_{PA} , and \dot{I}_{PA} is its derivative. Unlike the original input correlation rule, this rule uses soft weight bounding to avoid weights changing signs. Moreover, the sum of the weights was kept close to a ω_s value. In practice this meant dividing the each individual w value by the sum of weights from A -to- M connections, and multiplying times ω_s at each update. In addition, weight clipping was used to keep individual weights below a value ω_{max} .

The supplementary discussion (section 6.2) elaborates on how such a learning rule could be present in the spinal cord.

4.3 Exploratory mechanism

Without any additional mechanisms the model risked getting stuck in a fixed arm position before it could learn. We included two mechanisms to permit exploration in the system. The first mechanism consists of intrinsic noise in the CE and CI interneurons, which causes low-amplitude oscillations in the arm. We have observed that intrinsic oscillations in the CE, CI units are also effective to allow learning (data not shown), but the option of intrinsic noise permits the use of simple sigmoidal units in C , and contributes to the discussion regarding the role of noise in neural computation.

The second mechanism for exploration consists of an additional unit, called ACT . This unit acted similarly to a leaky integrator of the total activity in S_{PA} , reflecting the total error. If the leaky integral of the S_{PA} activity crossed a threshold, then ACT would send a signal to all the CE and CI units, causing adaptation. The adaptation consisted of an inhibitory current that grew depending on the accumulated previous activity.

To model this, CE and CI units received an extra input I_{adapt} . When the input from the ACT unit was larger than 0.8, and $I_{adapt} < 0.2$, the value of I_{adapt} would be set to $(u_i^{slow})^2$. This is the square of a low-passed filtered version of u_i . More explicitly,

$$\tau_{slow} \dot{u}_i^{slow} = u_i - u_i^{slow}. \quad (12)$$

If the input from ACT was smaller than 0.8, or I_{adapt} became larger than 0.2, then I_{adapt} would decay towards zero:

$$\tau_{slow} \dot{I}_{adapt} = -I_{adapt}. \quad (13)$$

With this mechanism, if the arm got stuck then error would accumulate, leading to adaptation in the spinal interneurons. This would cause the most active interneurons to receive the most inhibition, shifting the “dominant” activities, and producing larger-amplitude exploratory oscillations.

When a new target is presented, *ACT* must reset its own activity back to a low value. Given our requirement to fully implement the controller using neural elements, we needed a way to detect changes in S_P . A unit denominated *CHG* can detect these changes using synapses that react to the derivative of the activity in S_P units. *CHG* was connected to *ACT* in order to reset its activity.

More precisely, when inputs from *CHG* were larger than 0.1, the activity of *ACT* had dynamics:

$$\dot{a}(t) = -40a(t). \quad (14)$$

Otherwise it had these dynamics:

$$\dot{a}(t) = a(t)(\sigma(I) - \theta_{ACT}), \text{ if } \sigma(I) < \theta_{ACT}, \quad (15)$$

$$\tau_{ACT}\dot{a}(t) = (\sigma(I) - \theta_{ACT})[1 - a(t) + \gamma\dot{\sigma}(I)], \text{ otherwise.} \quad (16)$$

As before, $\sigma(\cdot)$ is a sigmoidal function, and I is the scaled sum of inputs other than *CHG*. When $\sigma(I)$ is smaller than a threshold θ_{ACT} the value of a actually decreases, as this error is deemed small enough. When $\sigma(I) > \theta_{ACT}$ the activity increases, but the rate of increase is modulated by a rate of increase $\dot{\sigma}(I) \equiv \sigma(I) - \sigma(\tilde{I})$, where \tilde{I} is a low-pass filtered version of I . γ is a constant paramter.

CHG was a standard sigmoidal unit receiving inputs from S_P , with each synaptic weight obeying this equation:

$$\omega_j(t) = \alpha|\dot{s}_j(t)| - \omega_j(t), \quad (17)$$

where s_j represents the synapse’s presynaptic input.

4.4 Plant, muscles, afferents

The planar arm was modelled as a compound double pendulum, where both the arm and forearm were cylinders with 1 kg. of mass. No gravity was present, and a moderate amount of viscous friction was added at each joint ($3 \frac{N \cdot m \cdot s}{rad}$). The derivation and validation of the double pendulum’s equations can be consulted in a Jupyter notebook included with Draculab’s source code (in the `tests` folder).

The muscles used a standard Hill-type model, as described in [7], Pg. 99. The muscle’s tension T obeys:

$$\dot{T} = \frac{K_{SE}}{b} \left[g \cdot I + K_{PE}\Delta x + b\dot{x} - \left(1 + \frac{K_{PE}}{K_{SE}} \right) T \right], \quad (18)$$

where I is the input, g an input gain, K_{PE} the parallel elasticity constant, K_{SE} the series elasticity constant, b is the damping constant for the parallel element, x is the length of the muscle, and $\Delta x = x - x_1^* - x_2^*$. In here, x_1^* is the resting length of the series element, whereas x_2^* is the resting length of the parallel

element. All resting lengths were calculated from the steady state when the hand was located at coordinates (0.3, 0.3).

We created a model of the Ia and II afferents using simple structural elements. This model includes, for each muscle one dynamic nuclear bag fiber, and one static bag fiber. Both of these fibers use the same tension equation as the muscle, but with different parameters. For the static bag fiber:

$$\dot{T}^s = \frac{K_{SE}^s}{b^s} \left[K_{PE}^s \Delta x + b^s \dot{x} - \left(1 + \frac{K_{PE}^s}{K_{SE}^s} \right) T^s \right]. \quad (19)$$

The dynamic bag fiber uses the same equation, with the s superscript replaced by d . No inputs were applied to the static or dynamic bag fibers, so they were removed from these equations. The rest lengths of the static and dynamic bag fibers were those of their corresponding muscles times factors l_0^s, l_0^d , respectively.

The Ia afferent output is proportional to a linear combination of the lengths for the serial elements in both dynamic and static bag fibers. The II output has two components, one proportional to the length of the serial element, and one approximately proportional to the length of the parallel element, both in the static bag fiber. In practice this was implemented through the following equations:

$$I_a = g_{I_a} \left[\left(\frac{f_s^{I_a}}{K_{SE}^s} \right) T^s + \left(\frac{1 - f_s^{I_a}}{K_{SE}^d} \right) T^d \right], \quad (20)$$

$$II = g_{II} \left[\left(\frac{f_s^{II}}{K_{SE}^s} \right) T^s + \left(\frac{1 - f_s^{II}}{K_{PE}^s} \right) (T^s - b^s \dot{x}) \right]. \quad (21)$$

In here, g_{I_a} and g_{II} are gain factors. $f_s^{I_a}$ and f_s^{II} are constants determining the fraction of I_a and II output that comes from the serial element.

The model of the Golgi tendon organ producing the Ib outputs was taken from [90]. First, a rectified tension was obtained as:

$$r = g_{I_b} \log(T^+ / T_0 + 1). \quad (22)$$

g_{I_b} is a gain factor, T_0 is a constant that can further alter the slope of the tension, and $T^+ = \max(T, 0)$ is the tension, half-rectified. The I_b afferent output followed dynamics:

$$\tau_{I_b} \dot{I}_b = r - I_b. \quad (23)$$

4.5 Synergistic network

We produced a version of the model where the units of activation consisted of pairs of muscles. As illustrated in figure 9, from the set of 6 muscles there are 15 combinations of 2 muscles, but 3 of them consist of antagonist pairs. Removing these we are left with 12 pairs of muscles, and for each muscle pair we had a Wilson-Cowan-like CE, CI pair sending projections to both of them. Furthermore, for each pair of muscles, there is another pair that contains both

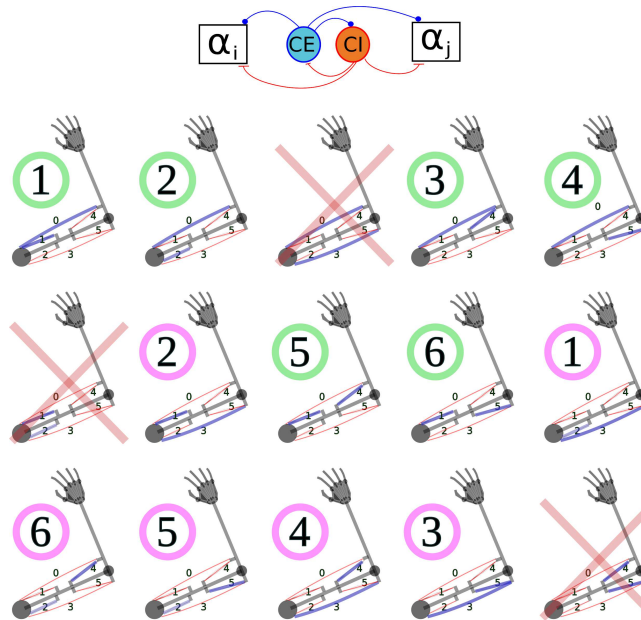


Figure 9: Modified architecture of the C population. Each pair of CE , CI units projects to two α motoneurons (top). There are 15 possible pairs of muscles, corresponding to the blue lines for each arm in the figure. Three of the pairs (marked with red crosses) contain antagonist muscles, and are not included. The remaining 12 pairs can be arranged into 2 groups of 6 units each. The units in the group marked with green circles are the antagonists of the units with the same number, marked with pink circles.

their antagonists, and we can use this fact to generalize the concept of antagonists when interneurons project to several motoneurons. The CE units sent projections to the CI units of their antagonists. This organization allowed us to maintain the balance between excitation and inhibition in the network, along with the connectivity motifs used previously.

4.6 Parameter search

We kept all parameter values in a range where they still made biological sense. Parameter values that were not constrained by biological data were adjusted using a genetic algorithm, and particle swarm optimization.

The parameters used can affect the results in the paper. We chose parameters that minimized the error during the second half of the learning phase, which is agnostic to the other results.

4.7 Preferred direction vectors

Next we describe how PD vectors were obtained for the M units.

Let m_{jk} denote the firing rate of the j -th M unit when reaching for the k -th target, averaged over the first 2 seconds, and across reaches to the same target. We created a function $h_j : \mathbb{R}^2 \rightarrow \mathbb{R}$ that mapped the X,Y coordinates of each target to its corresponding m_{jk} value, but in the domain of h_j the coordinates were shifted so the center location was at the origin.

Next we approximated h_j with a plane, using the least squares method, and obtained a unit vector u_j normal to that plane, starting at the intersection of the z -axis and the plane, and pointing towards the XY plane. The PD vector was defined as the projection of u_j on the XY plane.

In order to predict the PD vectors, we first obtained for each muscle the “direction of maximum contraction,” verbally described in panel B of figure 5. More formally, let l_{ik} denote the length of the i -th muscle when the hand is at target k , and let l_i^0 denote its length when the hand is at the center location. With \bar{r}_k we denote the unit vector with base at the center location, pointing in the direction of the k -th target. The direction of maximum length change for the i -th muscle comes from the following vector sum:

$$\bar{v}_i = \sum_{k=1}^8 \left[\frac{l_i^0 - l_{ik}}{l_i^0} \right]_+ \bar{r}_k, \quad (24)$$

where $[x]_+ = \max(x, 0)$.

For the j -th unit in M , its predicted PD vector comes from a linear combination of the \bar{v}_i vectors. Let the input to this unit be $\sum_i w_{ji} e_i$, where e_i is the output of the i -th SPF unit (representing the error in the i -th muscle). The predicted PD vector is:

$$\bar{d}_j = \sum_{i=0}^5 w_{ji} \bar{v}_i \quad (25)$$

4.8 Statistical tests

To find whether M units were significantly tuned to the reach direction we used a bootstrap procedure. For each unit we obtained the length of its PD vector 10,000 times when the identity of the target for each reach was randomly shuffled. We considered there was significant tuning when the length of the true PD vector was longer than 99.9% of these random samples.

To obtain the coefficient of determination for the predicted PD angles, let θ_{true}^j denote the angle of the true PD for the j -th M unit, and θ_{pred}^j be the angle of its predicted PD. We obtained residuals for the angles as $\epsilon_j = \theta_{true}^j - \theta_{pred}^j$, where this difference is actually the angle of the smallest rotation that turns one angle into the other. Each residual was then scaled by the norm of its corresponding PD vector, to account for the fact that these were not homogeneous. Denoting these scaled residuals as ϵ_j^* the residual sum of squares

is $SS_{res} = \sum_j (\epsilon_j^*)^2$. The total sum of squares was: $SS_{tot} = \sum_j (\theta_{true}^j - \bar{\theta}_{true})^2$, where $\bar{\theta}_{true}$ is the mean of the θ_{true}^j angles. The coefficient of determination comes from the usual formula $R^2 = 1 - \frac{SS_{res}}{SS_{tot}}$.

To assess bimodality of the PD distribution we used a version of the Rayleigh statistic adapted to look for bimodal distributions where the two modes are oriented at 180 degrees from each other, introduced in [82]. This test consists of finding an modified Rayleigh r statistic defined as:

$$r = \frac{1}{N} \left(\left(\sum_{i=1}^N \cos(2\phi_i) \right)^2 + \left(\sum_{i=1}^N \sin(2\phi_i) \right)^2 \right), \quad (26)$$

where the ϕ_i angles are the angles for the PDs. A bootstrap procedure is then used, where this r statistic is produced 100,000 times by sampling from the uniform distribution on the $(0, 1\pi)$ interval. The PD distribution was deemed significantly bimodal if its r value was larger than 99.9% of the random r values.

We used a bootstrap test to find whether there was statistical significance to the linear addition of direction fields. To make this independent of the individual pair of locations stimulated, we obtained the direction fields for all 15 possible pairs of locations, and for each pair calculated the mean angle difference between $D(a+b)$ and $D(a)+D(b)$ as described in the main text. We next obtained the mean of these 15 average angle deviations, to obtain a global average angle deviation γ_{global} .

We then repeated this procedure 400 times when the identities of the stimulation sites a, b were shuffled, to obtain 400 global average angle deviations γ_{global}^j . We declared statistical significance if γ_{global} was smaller than 99% of the γ_{global}^j values.

4.9 Connections from S_{PA} to M

When connections from S_{PA} to M were one-to-one, the j -th unit in S_{PA} only sent a projection to unit j in M .

In the other type of connectivity used in this paper, each M unit received a linear combination of S_{PA} inputs. The connectivity matrix for this case was based on the following 6-dimensional orthogonal matrix:

$$R = \begin{bmatrix} 1 & 1 & 1 & 1 & 1 & 1 \\ 1 & 1 & 1 & -1 & -1 & -1 \\ 1 & -2 & 1 & -1 & 2 & -1 \\ -1 & -1 & 2 & 2 & -1 & -1 \\ -1 & 1 & 0 & 0 & 1 & -1 \\ -1 & 0 & 1 & -1 & 0 & 1 \end{bmatrix}. \quad (27)$$

The rows of this matrix form an orthogonal basis in \mathfrak{R}^6 , and normalizing each row we obtain a matrix R^* whose rows form an orthonormal basis. Connections

from the 12 S_{PA} units to the 12 M units used this 12×12 matrix:

$$\begin{bmatrix} R^* & -R^* \\ -R^* & R^* \end{bmatrix}. \quad (28)$$

5 Acknowledgements

The authors wish to thank Prof. Kenji Doya for helping revise early versions of this manuscript.

References

- [1] Kaas, J. H. & Collins, C. E. *The Primate Visual System* (CRC Press, 2003). Google-Books-ID: rRu38JwnZXoC.
- [2] Ballard, D. H. & Zhang, R. The Hierarchical Evolution in Human Vision Modeling. *Topics in Cognitive Science* **13**, 309–328 (2021). URL <https://onlinelibrary.wiley.com/doi/abs/10.1111/tops.12527>. eprint: <https://onlinelibrary.wiley.com/doi/pdf/10.1111/tops.12527>.
- [3] Chersi, F. & Burgess, N. The Cognitive Architecture of Spatial Navigation: Hippocampal and Striatal Contributions. *Neuron* **88**, 64–77 (2015). URL <https://www.sciencedirect.com/science/article/pii/S0896627315007783>.
- [4] Moser, E. I., Moser, M.-B. & McNaughton, B. L. Spatial representation in the hippocampal formation: a history. *Nature Neuroscience* **20**, 1448–1464 (2017). URL <https://www.nature.com/articles/nn.4653>. Bandiera_abtest: a Cg_type: Nature Research Journals Number: 11 Primary_atype: Comments & Opinion Publisher: Nature Publishing Group Subject_term: Hippocampus;Spatial memory Subject_term_id: hippocampus;spatial-memory.
- [5] Eccles, J. C. Physiology of Motor Control in Man. *Stereotactic and Functional Neurosurgery* **44**, 5–15 (1981). URL <https://www.karger.com/Article/FullText/102178>. Publisher: Karger Publishers.
- [6] Loeb, G. E. & Tsianos, G. A. Major remaining gaps in models of sensorimotor systems. *Frontiers in Computational Neuroscience* **9** (2015). URL <https://www.frontiersin.org/articles/10.3389/fncom.2015.00070/full>. Publisher: Frontiers.
- [7] Shadmehr, R. & Wise, S. P. *The Computational Neurobiology of Reaching and Pointing: A Foundation for Motor Learning* (MIT Press, 2005). Google-Books-ID: fKelmql1s_sC.

- [8] Arber, S. & Costa, R. M. Connecting neuronal circuits for movement. *Science* **360**, 1403–1404 (2018). URL <https://www.science.org/lookup/doi/10.1126/science.aat5994>. Publisher: American Association for the Advancement of Science.
- [9] Tanaka, Y. H. *et al.* Thalamocortical Axonal Activity in Motor Cortex Exhibits Layer-Specific Dynamics during Motor Learning. *Neuron* **100**, 244–258.e12 (2018). URL <https://www.sciencedirect.com/science/article/pii/S0896627318306895>.
- [10] Hadders-Algra, M. Early human motor development: From variation to the ability to vary and adapt. *Neuroscience & Biobehavioral Reviews* **90**, 411–427 (2018). URL <https://www.sciencedirect.com/science/article/pii/S0149763418300538>.
- [11] Verduzco-Flores, S., Dorrell, W. & DeSchutter, E. An approach to synaptic learning for autonomous motor control. *arXiv:2006.13471 [nlin, q-bio]* (2021). URL <http://arxiv.org/abs/2006.13471>. ArXiv: 2006.13471.
- [12] Woods, S. C. & Ramsay, D. S. Homeostasis: Beyond Curt Richter. *Appetite* **49**, 388–398 (2007). URL <https://www.sciencedirect.com/science/article/pii/S019566630700270X>.
- [13] Doya, K., Kimura, H. & Kawato, M. Neural mechanisms of learning and control. *IEEE Control Systems* **21**, 42–54 (2001).
- [14] Merel, J., Botvinick, M. & Wayne, G. Hierarchical motor control in mammals and machines. *Nature Communications* **10**, 1–12 (2019). URL <https://www.nature.com/articles/s41467-019-13239-6>.
- [15] Bizzi, E., Tresch, M. C., Saltiel, P. & d’Avella, A. New perspectives on spinal motor systems. *Nature Reviews Neuroscience* **1**, 101–108 (2000). URL <https://www.nature.com/articles/35039000>.
- [16] Lemon, R. N. Descending Pathways in Motor Control. *Annual Review of Neuroscience* **31**, 195–218 (2008). URL <https://www.annualreviews.org/doi/10.1146/annurev.neuro.31.060407.125547>.
- [17] Arber, S. Motor Circuits in Action: Specification, Connectivity, and Function. *Neuron* **74**, 975–989 (2012). URL <http://www.sciencedirect.com/science/article/pii/S0896627312004771>.
- [18] Asante, C. O. & Martin, J. H. Differential Joint-Specific Corticospinal Tract Projections within the Cervical Enlargement. *PLOS ONE* **8**, e74454 (2013). URL <https://journals.plos.org/plosone/article?id=10.1371/journal.pone.0074454>.
- [19] Alstermark, B. & Isa, T. Circuits for Skilled Reaching and Grasping. *Annual Review of Neuroscience* **35**, 559–578 (2012). URL <https://doi.org/10.1146/annurev-neuro-062111-150527>.

- [20] Jankowska, E. Spinal Interneurons. In Pfaff, D. W. (ed.) *Neuroscience in the 21st Century: From Basic to Clinical*, 1063–1099 (Springer, New York, NY, 2013). URL <https://doi.org/10.1007/978-1-4614-1997-634>.
- [21] Wang, X. *et al.* Deconstruction of Corticospinal Circuits for Goal-Directed Motor Skills. *Cell* **171**, 440–455.e14 (2017). URL <http://www.sciencedirect.com/science/article/pii/S009286741730939X>.
- [22] Ueno, M. *et al.* Corticospinal Circuits from the Sensory and Motor Cortices Differentially Regulate Skilled Movements through Distinct Spinal Interneurons. *Cell Reports* **23**, 1286–1300.e7 (2018). URL <http://www.sciencedirect.com/science/article/pii/S2211124718305254>.
- [23] Wolpaw, J. R., Kieffer, V. A., Seegal, R. F., Braitman, D. J. & Sanders, M. G. Adaptive plasticity in the spinal stretch reflex. *Brain Research* **267**, 196–200 (1983). URL <https://www.sciencedirect.com/science/article/pii/0006899383910594>.
- [24] Grau, J. W. Learning from the spinal cord: How the study of spinal cord plasticity informs our view of learning. *Neurobiology of Learning and Memory* **108**, 155–171 (2014). URL <https://www.sciencedirect.com/science/article/pii/S1074742713001445>.
- [25] Meyer-Lohmann, J., Christakos, C. N. & Wolf, H. Dominance of the short-latency component in perturbation induced electromyographic responses of long-trained monkeys. *Experimental Brain Research* **64**, 393–399 (1986). URL <https://doi.org/10.1007/BF00340475>.
- [26] Wolpaw, J. R. The complex structure of a simple memory. *Trends in Neurosciences* **20**, 588–594 (1997). URL <http://www.sciencedirect.com/science/article/pii/S0166223697011338>.
- [27] Norton, J. J. & Wolpaw, J. R. Acquisition, maintenance, and therapeutic use of a simple motor skill. *Current Opinion in Behavioral Sciences* **20**, 138–144 (2018). URL <http://www.sciencedirect.com/science/article/pii/S235215461730219X>.
- [28] Georgopoulos, A., Kalaska, J., Caminiti, R. & Massey, J. On the relations between the direction of two-dimensional arm movements and cell discharge in primate motor cortex. *The Journal of Neuroscience* **2**, 1527–1537 (1982). URL <https://www.ncbi.nlm.nih.gov/pmc/articles/PMC6564361/>.
- [29] Georgopoulos, A. P., Schwartz, A. B. & Kettner, R. E. Neuronal population coding of movement direction. *Science* **233**, 1416–1419 (1986). URL <https://science.sciencemag.org/content/233/4771/1416>. Publisher: American Association for the Advancement of Science Section: Reports.

- [30] Kakei, S., Hoffman, D. S. & Strick, P. L. Muscle and Movement Representations in the Primary Motor Cortex. *Science* (1999). URL <https://www.science.org/doi/abs/10.1126/science.285.5436.2136>. Publisher: American Association for the Advancement of Science.
- [31] Truccolo, W., Friehs, G. M., Donoghue, J. P. & Hochberg, L. R. Primary Motor Cortex Tuning to Intended Movement Kinematics in Humans with Tetraplegia. *Journal of Neuroscience* **28**, 1163–1178 (2008). URL <https://www.jneurosci.org/content/28/5/1163>. Publisher: Society for Neuroscience Section: Articles.
- [32] Kalaska, J. F. From intention to action: motor cortex and the control of reaching movements. *Advances in Experimental Medicine and Biology* **629**, 139–178 (2009).
- [33] Georgopoulos, A. P. & Stefanis, C. N. Local shaping of function in the motor cortex: Motor contrast, directional tuning. *Brain Research Reviews* **55**, 383–389 (2007). URL <https://www.sciencedirect.com/science/article/pii/S0165017307000720>.
- [34] Harrison, T. C. & Murphy, T. H. Towards a circuit mechanism for movement tuning in motor cortex. *Frontiers in Neural Circuits* **6** (2013). URL <https://www.frontiersin.org/articles/10.3389/fncir.2012.00127/full>. Publisher: Frontiers.
- [35] Tanaka, H. Modeling the motor cortex: Optimality, recurrent neural networks, and spatial dynamics. *Neuroscience Research* **104**, 64–71 (2016). URL <https://www.sciencedirect.com/science/article/pii/S0168010215002631>.
- [36] Morrow, M. M. & Miller, L. E. Prediction of Muscle Activity by Populations of Sequentially Recorded Primary Motor Cortex Neurons. *Journal of Neurophysiology* **89**, 2279–2288 (2003). URL <https://journals.physiology.org/doi/full/10.1152/jn.00632.2002>. Publisher: American Physiological Society.
- [37] Todorov, E. Direct cortical control of muscle activation in voluntary arm movements: a model. *Nature Neuroscience* **3**, 391–398 (2000). URL https://www.nature.com/articles/nn0400_391.
- [38] Scott, S. H., Gribble, P. L., Graham, K. M. & Cabel, D. W. Dissociation between hand motion and population vectors from neural activity in motor cortex. *Nature* **413**, 161–165 (2001). URL <https://www.nature.com/articles/35093102>.
- [39] Rokni, U., Richardson, A. G., Bizzi, E. & Seung, H. S. Motor Learning with Unstable Neural Representations. *Neuron* **54**, 653–666 (2007). URL <https://www.sciencedirect.com/science/article/pii/S0896627307003339>.

- [40] Padoa-Schioppa, C., Li, C.-S. R. & Bizzi, E. Neuronal Activity in the Supplementary Motor Area of Monkeys Adapting to a New Dynamic Environment. *Journal of Neurophysiology* **91**, 449–473 (2004). URL <https://journals.physiology.org/doi/full/10.1152/jn.00876.2002>. Publisher: American Physiological Society.
- [41] Shenoy, K. V., Sahani, M. & Churchland, M. M. Cortical Control of Arm Movements: A Dynamical Systems Perspective. *Annual Review of Neuroscience* **36**, 337–359 (2013). URL <http://www.annualreviews.org/doi/10.1146/annurev-neuro-062111-150509>.
- [42] Sussillo, D., Churchland, M. M., Kaufman, M. T. & Shenoy, K. V. A neural network that finds a naturalistic solution for the production of muscle activity. *Nature Neuroscience* **18**, 1025–1033 (2015). URL <https://www.nature.com/articles/nn.4042>.
- [43] Churchland, M. *et al.* Neural population dynamics during reaching. *Nature* **487**, 51–56 (2012). URL <https://www.ncbi.nlm.nih.gov/pmc/articles/PMC3393826/>.
- [44] Schöner, G., Tekülve, J. & Zibner, S. Reaching for objects: a neural process account in a developmental perspective. In *Reach-to-Grasp Behavior*, 281–318 (Routledge, 2018).
- [45] Valero-Cuevas, F. J. A mathematical approach to the mechanical capabilities of limbs and fingers. *Advances in Experimental Medicine and Biology* **629**, 619–633 (2009).
- [46] Keener, J. P. *Principles Of Applied Mathematics: Transformation And Approximation* (Avalon Publishing, 1995). Google-Books-ID: 5nlQAAAA-MAAJ.
- [47] Giszter, S. F. Motor primitives: new data and future questions. *Current Opinion in Neurobiology* **33**, 156–165 (2015). URL <http://www.sciencedirect.com/science/article/pii/S095943881500077X>.
- [48] Mussa-Ivaldi, F. A. & Bizzi, E. Motor Learning through the Combination of Primitives. *Philosophical Transactions: Biological Sciences* **355**, 1755–1769 (2000). URL <https://www.jstor.org/stable/3066920>. Publisher: The Royal Society.
- [49] Bizzi, E., Mussa-Ivaldi, F. A. & Giszter, S. Computations underlying the execution of movement: a biological perspective. *Science* **253**, 287–291 (1991). URL <https://science.sciencemag.org/content/253/5017/287>. Publisher: American Association for the Advancement of Science Section: Articles.

- [50] Kelso, J. A. S. Synergies: Atoms of Brain and Behavior. In Sternad, D. (ed.) *Progress in Motor Control: A Multidisciplinary Perspective*, Advances in Experimental Medicine and Biology, 83–91 (Springer US, Boston, MA, 2009). URL https://doi.org/10.1007/978-0-387-77064-2_5.
- [51] Bruton, M. & ODwyer, N. Synergies in coordination: a comprehensive overview of neural, computational, and behavioral approaches. *Journal of Neurophysiology* **120**, 2761–2774 (2018). URL <https://journals.physiology.org/doi/full/10.1152/jn.00052.2018>. Publisher: American Physiological Society.
- [52] Giszter, S. F., Mussa-Ivaldi, F. A. & Bizzi, E. Convergent force fields organized in the frog’s spinal cord. *Journal of Neuroscience* **13**, 467–491 (1993). URL <https://www.jneurosci.org/content/13/2/467>. Publisher: Society for Neuroscience Section: Articles.
- [53] Mussa-Ivaldi, F. A., Giszter, S. F. & Bizzi, E. Linear combinations of primitives in vertebrate motor control. *Proceedings of the National Academy of Sciences* **91**, 7534–7538 (1994). URL <https://www.pnas.org/content/91/16/7534>. Publisher: National Academy of Sciences Section: Research Article.
- [54] Tresch, M. C. & Jarc, A. The case for and against muscle synergies. *Current Opinion in Neurobiology* **19**, 601–607 (2009). URL <https://www.sciencedirect.com/science/article/pii/S095943880900124X>.
- [55] de Rugy, A., Loeb, G. & Carroll, T. Are muscle synergies useful for neural control? *Frontiers in Computational Neuroscience* **0** (2013). URL <https://www.frontiersin.org/articles/10.3389/fncom.2013.00019/full>. Publisher: Frontiers.
- [56] Bizzi, E. & Cheung, V. C. The neural origin of muscle synergies. *Frontiers in Computational Neuroscience* **7** (2013). URL <https://www.frontiersin.org/articles/10.3389/fncom.2013.00051/full>. Publisher: Frontiers.
- [57] Levine, A. J. *et al.* Identification of a cellular node for motor control pathways. *Nature neuroscience* **17**, 586–593 (2014). URL <https://www.ncbi.nlm.nih.gov/pmc/articles/PMC4569558/>.
- [58] Pulvermüller, F., Tomasello, R., Henningsen-Schomers, M. R. & Wennekers, T. Biological constraints on neural network models of cognitive function. *Nature Reviews Neuroscience* 1–15 (2021). URL <https://www.nature.com/articles/s41583-021-00473-5>. Bandiera_abtest: a Cg_type: Nature Research Journals Primary_atype: Reviews Publisher: Nature Publishing Group Subject_term: Cognitive neuroscience;Human behaviour;Network models Subject_term_id: cognitive-neuroscience;human-behaviour;network-models.

- [59] O'Reilly, R. C. Six principles for biologically based computational models of cortical cognition. *Trends in Cognitive Sciences* **2**, 455–462 (1998). URL <http://www.sciencedirect.com/science/article/pii/S1364661398012418>.
- [60] Richards, B. A. *et al.* A deep learning framework for neuroscience. *Nature Neuroscience* **22**, 1761–1770 (2019). URL <https://www.nature.com/articles/s41593-019-0520-2>. Bandiera_abtest: a Cg_type: Nature Research Journals Number: 11 Primary_atype: Reviews Publisher: Nature Publishing Group Subject_term: Learning algorithms;Machine learning;Neural circuits Subject_term_id: learning-algorithms;machine-learning;neural-circuit.
- [61] Powers, W. T. Feedback: Beyond Behaviorism Stimulus-response laws are wholly predictable within a control-system model of behavioral organization. *Science* **179**, 351–356 (1973). URL <http://www.sciencemag.org/content/179/4071/351>.
- [62] Powers, W. T. *Behavior: The Control of Perception (2nd ed. rev. & exp.)*, vol. xiv (Benchmark Press, New Canaan, CT, US, 2005).
- [63] Adams, R. A., Shipp, S. & Friston, K. J. Predictions not commands: active inference in the motor system. *Brain Structure and Function* **218**, 611–643 (2013). URL <http://link.springer.com/10.1007/s00429-012-0475-5>.
- [64] Miri, A., Azim, E. & Jessell, T. M. Edging toward Entelechy in Motor Control. *Neuron* **80**, 827–834 (2013). URL [https://www.cell.com/neuron/abstract/S0896-6273\(13\)01001-5](https://www.cell.com/neuron/abstract/S0896-6273(13)01001-5). Publisher: Elsevier.
- [65] Tsianos, G. A., Goodner, J. & Loeb, G. E. Useful properties of spinal circuits for learning and performing planar reaches. *Journal of Neural Engineering* **11**, 056006 (2014). URL <https://doi.org/10.1088%2F1741-2560%2F11%2F5%2F056006>.
- [66] Mileusnic, M. P., Brown, I. E., Lan, N. & Loeb, G. E. Mathematical Models of Proprioceptors. I. Control and Transduction in the Muscle Spindle. *Journal of Neurophysiology* **96**, 1772–1788 (2006). URL <https://www.physiology.org/doi/10.1152/jn.00868.2005>.
- [67] Mountcastle, V. B. The columnar organization of the neocortex. *Brain* **120**, 701–722 (1997). URL <https://academic.oup.com/brain/article/120/4/701/372118>.
- [68] Porr, B. & Wörgötter, F. Strongly Improved Stability and Faster Convergence of Temporal Sequence Learning by Using Input Correlations Only. *Neural Computation* **18**, 1380–1412 (2006). URL <https://doi.org/10.1162/neco.2006.18.6.1380>.

- [69] Shafi, M. *et al.* Variability in neuronal activity in primate cortex during working memory tasks. *Neuroscience* **146**, 1082–1108 (2007). URL <http://www.sciencedirect.com/science/article/pii/S0306452206017593>.
- [70] Steinmetz, N. A., Zatzka-Haas, P., Carandini, M. & Harris, K. D. Distributed coding of choice, action and engagement across the mouse brain. *Nature* **576**, 266–273 (2019). URL <https://www.nature.com/articles/s41586-019-1787-x>. Number: 7786 Publisher: Nature Publishing Group.
- [71] Najafi, F. *et al.* Excitatory and Inhibitory Subnetworks Are Equally Selective during Decision-Making and Emerge Simultaneously during Learning. *Neuron* **105**, 165–179.e8 (2020). URL <https://www.sciencedirect.com/science/article/pii/S0896627319308487>.
- [72] Berg, R. W., Willumsen, A. & Lindn, H. When networks walk a fine line: balance of excitation and inhibition in spinal motor circuits. *Current Opinion in Physiology* **8**, 76–83 (2019). URL <https://www.sciencedirect.com/science/article/pii/S2468867319300069>.
- [73] Goulding, M., Bourane, S., Garcia-Campmany, L., Dalet, A. & Koch, S. Inhibition downunder: an update from the spinal cord. *Current Opinion in Neurobiology* **26**, 161–166 (2014). URL <http://www.sciencedirect.com/science/article/pii/S0959438814000567>.
- [74] Cowan, J. D., Neuman, J. & van Drongelen, W. Wilson-Cowan Equations for Neocortical Dynamics. *The Journal of Mathematical Neuroscience* **6**, 1 (2016). URL <https://doi.org/10.1186/s13408-015-0034-5>.
- [75] Pierrot-Deseilligny, E. & Burke, D. *The Circuitry of the Human Spinal Cord: Its Role in Motor Control and Movement Disorders* (Cambridge University Press, Cambridge, 2005). URL <https://www.cambridge.org/core/books/circuitry-of-the-human-spinal-cord/BBDFC31B44453B>
- [76] Kaufman, M. T., Churchland, M. M., Ryu, S. I. & Shenoy, K. V. Cortical activity in the null space: permitting preparation without movement. *Nature Neuroscience* **17**, 440–448 (2014). URL <https://www.nature.com/articles/nn.3643>. Bandiera_abtest: a Cg.type: Nature Research Journals Number: 3 Primary_atype: Research Publisher: Nature Publishing Group Subject_term: Motor cortex; Premotor cortex Subject_term_id: motor-cortex; premotor-cortex.
- [77] Gilman, S., Carr, D. & Hollenberg, J. Kinematic effects of deafferentation and cerebellar ablation. *Brain* **99**, 311–330 (1976). URL <https://doi.org/10.1093/brain/99.2.311>.
- [78] Bizzi, E. & Ajemian, R. From motor planning to execution: a sensorimotor loop perspective. *Journal of Neurophysiology* **124**, 1815–1823 (2020). URL <https://journals.physiology.org/doi/full/10.1152/jn.00715.2019>. Publisher: American Physiological Society.

- [79] Bastian, A. J., Martin, T. A., Keating, J. G. & Thach, W. T. Cerebellar ataxia: abnormal control of interaction torques across multiple joints. *Journal of Neurophysiology* **76**, 492–509 (1996). URL <https://journals.physiology.org/doi/abs/10.1152/jn.1996.76.1.492>. Publisher: American Physiological Society.
- [80] Becker, W. J., Morrice, B. L., Clark, A. W. & Lee, R. G. Multi-Joint Reaching Movements and Eye-Hand Tracking in Cerebellar Incoordination: Investigation of a Patient with Complete Loss of Purkinje Cells. *Canadian Journal of Neurological Sciences* **18**, 476–487 (1991). URL <https://www.cambridge.org/core/journals/canadian-journal-of-neurological-sciences/article>. Publisher: Cambridge University Press.
- [81] Day, B. L., Thompson, P. D., Harding, A. E. & Marsden, C. D. Influence of vision on upper limb reaching movements in patients with cerebellar ataxia. *Brain* **121**, 357–372 (1998). URL <https://doi.org/10.1093/brain/121.2.357>.
- [82] Lillicrap, T. & Scott, S. Preference Distributions of Primary Motor Cortex Neurons Reflect Control Solutions Optimized for Limb Biomechanics. *Neuron* **77**, 168–179 (2013). URL <http://www.sciencedirect.com/science/article/pii/S0896627312009920>.
- [83] Kurtzer, I., Pruszynski, J. A., Herter, T. M. & Scott, S. H. Primate Upper Limb Muscles Exhibit Activity Patterns That Differ From Their Anatomical Action During a Postural Task. *Journal of Neurophysiology* **95**, 493–504 (2006). URL <https://journals.physiology.org/doi/full/10.1152/jn.00706.2005>. Publisher: American Physiological Society.
- [84] Chambers, A. R. & Rumpel, S. A stable brain from unstable components: Emerging concepts and implications for neural computation. *Neuroscience* **357**, 172–184 (2017). URL <http://www.sciencedirect.com/science/article/pii/S0306452217304013>.
- [85] Kalidindi, H. T. *et al.* Rotational dynamics in motor cortex are consistent with a feedback controller. *eLife* **10**, e67256 (2021). URL <https://doi.org/10.7554/eLife.67256>. Publisher: eLife Sciences Publications, Ltd.
- [86] DeWolf, T., Stewart, T. C., Slotine, J.-J. & Eliasmith, C. A spiking neural model of adaptive arm control. *Proceedings of the Royal Society B: Biological Sciences* (2016). URL <https://royalsocietypublishing.org/doi/abs/10.1098/rspb.2016.2134>. Publisher: The Royal Society.
- [87] Sanguineti, V. *et al.* Cerebellar ataxia: Quantitative assessment and cybernetic interpretation. *Human Movement Science* **22**, 189–205 (2003). URL <https://www.sciencedirect.com/science/article/pii/S0167945702001598>.

- [88] Richter, S. *et al.* Adaptive Motor Behavior of Cerebellar Patients During Exposure to Unfamiliar External Forces. *Journal of Motor Behavior* **36**, 28–38 (2004). URL <https://doi.org/10.3200/JMBR.36.1.28-38>. Publisher: Routledge eprint: <https://doi.org/10.3200/JMBR.36.1.28-38>.
- [89] Verduzco-Flores, S. & De Schutter, E. Draculab: A Python Simulator for Firing Rate Neural Networks With Delayed Adaptive Connections. *Frontiers in Neuroinformatics* **13** (2019). URL <https://www.frontiersin.org/articles/10.3389/fninf.2019.00018/full>.
- [90] Lin, C.-C. K. & Crago, P. E. Neural and Mechanical Contributions to the Stretch Reflex: A Model Synthesis. *Annals of Biomedical Engineering* **30**, 54–67 (2002). URL <https://doi.org/10.1114/1.1432692>.
- [91] Cheah, C. C., Liu, C. & Slotine, J. J. E. Adaptive Tracking Control for Robots with Unknown Kinematic and Dynamic Properties. *The International Journal of Robotics Research* **25**, 283–296 (2006). URL <https://doi.org/10.1177/0278364906063830>. Publisher: SAGE Publications Ltd STM.
- [92] Sanner, R. & Slotine, J.-J. Gaussian networks for direct adaptive control. *IEEE Transactions on Neural Networks* **3**, 837–863 (1992). Conference Name: IEEE Transactions on Neural Networks.
- [93] Bekolay, T. *et al.* Nengo: a Python tool for building large-scale functional brain models. *Frontiers in Neuroinformatics* **7** (2014). URL <https://www.frontiersin.org/articles/10.3389/fninf.2013.00048/full>.
- [94] Dura-Bernal, S. *et al.* Cortical Spiking Network Interfaced with Virtual Musculoskeletal Arm and Robotic Arm. *Frontiers in Neuroinformatics* **9**, 13 (2015). URL <https://www.frontiersin.org/article/10.3389/fninf.2015.00013>.
- [95] Li, W., Todorov, E. & Pan, X. Hierarchical Feedback and Learning for Multi-joint Arm Movement Control. In *2005 IEEE Engineering in Medicine and Biology 27th Annual Conference*, 4400–4403 (2005). ISSN: 1558-4615.
- [96] Martin, V., Scholz, J. P. & Schner, G. Redundancy, Self-Motion, and Motor Control. *Neural Computation* **21**, 1371–1414 (2009). URL <https://doi.org/10.1162/neco.2008.01-08-698>.
- [97] Caligiore, D., Parisi, D. & Baldassarre, G. Integrating reinforcement learning, equilibrium points, and minimum variance to understand the development of reaching: A computational model. *Psychological Review* **121**, 389–421 (2014). Place: US Publisher: American Psychological Association.
- [98] Sutton, R. S. & Barto, A. G. *Reinforcement Learning: An Introduction* (MIT Press, 2018). Google-Books-ID: sWV0DwAAQBAJ.

- [99] Feldman, A. G. Once More on the Equilibrium-Point Hypothesis (Model) for Motor Control. *Journal of Motor Behavior* **18**, 17–54 (1986). URL <https://doi.org/10.1080/00222895.1986.10735369>. Publisher: Routledge _eprint: <https://doi.org/10.1080/00222895.1986.10735369>.
- [100] Izawa, J., Kondo, T. & Ito, K. Biological arm motion through reinforcement learning. *Biological Cybernetics* **91**, 10–22 (2004). URL <https://doi.org/10.1007/s00422-004-0485-3>.
- [101] Mici, L., Parisi, G. I. & Wermter, S. An Incremental Self-Organizing Architecture for Sensorimotor Learning and Prediction. *IEEE Transactions on Cognitive and Developmental Systems* **10**, 918–928 (2018). Conference Name: IEEE Transactions on Cognitive and Developmental Systems.
- [102] Sussillo, D. & Abbott, L. F. Generating Coherent Patterns of Activity from Chaotic Neural Networks. *Neuron* **63**, 544–557 (2009). URL <https://www.sciencedirect.com/science/article/pii/S0896627309005479>.
- [103] Bashor, D. P. A large-scale model of some spinal reflex circuits. *Biological Cybernetics* **78**, 147–157 (1998). URL <https://doi.org/10.1007/s004220050421>.
- [104] Stienen, A. H. A., Schouten, A. C., Schuurmans, J. & van der Helm, F. C. T. Analysis of reflex modulation with a biologically realistic neural network. *Journal of Computational Neuroscience* **23**, 333 (2007). URL <https://doi.org/10.1007/s10827-007-0037-7>.
- [105] Cutsuridis, V. Does abnormal spinal reciprocal inhibition lead to co-contraction of antagonist motor units? a modeling study. *International Journal of Neural Systems* **17**, 319–327 (2007). URL <https://www.worldscientific.com/doi/abs/10.1142/S0129065707001160>. Publisher: World Scientific Publishing Co.
- [106] Cisi, R. R. L. & Kohn, A. F. Simulation system of spinal cord motor nuclei and associated nerves and muscles, in a Web-based architecture. *Journal of Computational Neuroscience* **25**, 520–542 (2008). URL <https://doi.org/10.1007/s10827-008-0092-8>.
- [107] Farina, D., Negro, F. & Dideriksen, J. L. The effective neural drive to muscles is the common synaptic input to motor neurons. *The Journal of Physiology* **592**, 3427–3441 (2014). URL <https://physoc.onlinelibrary.wiley.com/doi/abs/10.1113/jphysiol.2014.273581>. _eprint: <https://physoc.onlinelibrary.wiley.com/doi/pdf/10.1113/jphysiol.2014.273581>.
- [108] Shevtsova, N. A. *et al.* Organization of leftright coordination of neuronal activity in the mammalian spinal cord: Insights from computational modelling. *The Journal of Physiology* **593**, 2403–2426 (2015). URL <https://physoc.onlinelibrary.wiley.com/doi/abs/10.1113/JP270121>. _eprint: <https://physoc.onlinelibrary.wiley.com/doi/pdf/10.1113/JP270121>.

- [109] Shevtsova, N. A. & Rybak, I. A. Organization of flexorextensor interactions in the mammalian spinal cord: insights from computational modelling. *The Journal of Physiology* **594**, 6117–6131 (2016). URL <https://www.ncbi.nlm.nih.gov/pmc/articles/PMC5088238/>.
- [110] Danner, S. M., Shevtsova, N. A., Frigon, A. & Rybak, I. A. Computational modeling of spinal circuits controlling limb coordination and gaits in quadrupeds. *eLife* **6**, e31050 (2017). URL <https://doi.org/10.7554/eLife.31050>. Publisher: eLife Sciences Publications, Ltd.
- [111] Zelenin, P. V. *et al.* Differential Contribution of V0 Interneurons to Execution of Rhythmic and Nonrhythmic Motor Behaviors. *The Journal of Neuroscience: The Official Journal of the Society for Neuroscience* **41**, 3432–3445 (2021).
- [112] Stachowski, N. J. & Dougherty, K. J. Spinal Inhibitory Interneurons: Gatekeepers of Sensorimotor Pathways. *International Journal of Molecular Sciences* **22**, 2667 (2021). URL <https://www.ncbi.nlm.nih.gov/pmc/articles/PMC7961554/>.
- [113] Borisyuk, R., Azad, A., Conte, D., Roberts, A. & Soffe, S. Modeling the Connectome of a Simple Spinal Cord. *Frontiers in Neuroinformatics* **5**, 20 (2011). URL <https://www.frontiersin.org/article/10.3389/fninf.2011.00020>.
- [114] Cangiano, L. & Grillner, S. Mechanisms of Rhythm Generation in a Spinal Locomotor Network Deprived of Crossed Connections: The Lamprey Hemicord. *Journal of Neuroscience* **25**, 923–935 (2005). URL <https://www.jneurosci.org/content/25/4/923>. Publisher: Society for Neuroscience Section: Behavioral/Systems/Cognitive.
- [115] Zappacosta, S., Mannella, F., Mirolli, M. & Baldassarre, G. General differential Hebbian learning: Capturing temporal relations between events in neural networks and the brain. *PLOS Computational Biology* **14**, e1006227 (2018). URL <https://journals.plos.org/ploscompbiol/article?id=10.1371/journal.pcbi.1006227>. Publisher: Public Library of Science.
- [116] Fiete, I. R., Senn, W., Wang, C. Z. H. & Hahnloser, R. H. R. Spike-Time-Dependent Plasticity and Heterosynaptic Competition Organize Networks to Produce Long Scale-Free Sequences of Neural Activity. *Neuron* **65**, 563–576 (2010). URL <https://www.sciencedirect.com/science/article/pii/S0896627310000917>.
- [117] Kaleb, K., Pedrosa, V. & Clopath, C. Network-centered homeostasis through inhibition maintains hippocampal spatial map and cortical circuit function. *Cell Reports* **36**, 109577 (2021). URL <https://www.sciencedirect.com/science/article/pii/S2211124721010111>.

- [118] Lim, S. & Goldman, M. S. Balanced cortical microcircuitry for maintaining information in working memory. *Nature Neuroscience* **16**, 1306–1314 (2013). URL <https://www.nature.com/articles/nn.3492>. Bandiera_abtest: a Cg_type: Nature Research Journals Number: 9 Primary_atype: Research Publisher: Nature Publishing Group Subject_term: Network models Subject_term_id: network-models.
- [119] Helmchen, F. Dendrites as biochemical compartments. In *Dendrites*, 376 (Oxford University Press, Oxford, England, 1999). URL https://pure.mpg.de/pubman/faces/ViewItemOverviewPage.jsp?itemId=item_2537436.
- [120] Sar, P. & Geyer, H. A model for the transfer of control from the brain to the spinal cord through synaptic learning. *Journal of Computational Neuroscience* **48**, 365–375 (2020). URL <https://doi.org/10.1007/s10827-020-00767-0>.
- [121] Kawato, M., Ohmae, S., Hoang, H. & Sanger, T. 50 years since the Marr, Ito, and Albus models of the cerebellum. *arXiv:2003.05647 [q-bio]* (2020). URL <http://arxiv.org/abs/2003.05647>. ArXiv: 2003.05647.

SUPPLEMENTAL INFORMATION

6 Supplemental Discussion

6.1 Comparison with previous models

There are many other models of reaching and motor control. Most of them have one or more of the following limitations:

1. They use non-neural systems to produce motor commands.
2. They control a single degree of freedom, sidestepping the problem of controller configuration, since the error is one-dimensional.
3. They do not model a biologically plausible form of synaptic learning.

We will contrast our model with some of the work that does not strongly present these limitations, and with a few others. Due to space limitations, the contributions of many models will not be addressed, and, for those mentioned, we will limit ourselves to explain some of their limitations.

The model in [86] is similar has similar goals to our model, but with very different assumptions. In their model, motor cortex receives a location error vector x , and transforms it into a vector of joint torques. So that this transformation implements adaptive kinematics, it must approximate a Jacobian matrix that includes the effects of the arm’s inertia matrix, using location errors and joint velocities as training signals. This is accomplished by adapting an algorithm taken from the robotics literature [91], implementing it in a spiking

neural network. Additionally a second algorithm from robotics [92] is used to provide an adaptive dynamics component, which is interpreted as the cerebellar contributions.

In order to implement vector functions in spiking neural networks [86] uses the Neural Engineering Framework [93]. The essence of this approach is to represent values in populations of neurons with cosine-like tuning functions. These populations implement expansive recoding, becoming a massively overcomplete basis of the input space. Implementing a function using this population as the input is akin to using a linear decoder to extract the desired function values from the population activity. This can be done through standard methods, such as least-squares minimization, or random gradient descent. The parameters of the linear decoder then become weights of a feedforward neural layer implementing the function.

The model in [86] has therefore a rather different approach. They use engineering techniques to create a powerful motor control system, using algorithms from robotics, and 30,000 neurons to approximate their computations, which are then ascribed to sensory, motor, and premotor cortices, as well as the cerebellum. In contrast, we use 74 firing rate units, and unlike [86] we include muscles, muscle afferents, transmission delays, and a spinal cord.

There is nothing intrinsically wrong with using an engineering approach to try to understand a biological function. The crucial part is which model will be experimentally validated. Some differences between the models that may be able to separate them experimentally are: 1) In [86] premotor cortex is required to produce the error signal, whereas we ascribed this to sensory cortex. 2) In [86] direct afferent connections to motor cortex are not considered, whereas in our model they are necessary to maintain stability during learning (in the absence of a cerebellum). 3) In [86] spinal cord adaptation is not necessary to implement adaptive kinematics. In contrast, spinal cord adaptation is the basis of our model.

The model in [94] uses spiking neurons, and a realistic neuromechanical model in order to perform 2D reaching. The feedback is in term of muscle lengths, rather than muscle afferent signals. There is no mechanism to stop the arm, or hold it on target. Most importantly, learning relies on a critic, sending rewarding or punishing signals depending on whether the hand was approaching or getting away from the target. This is implicitly reducing the error dimension using a hidden mechanism. Furthermore, each single target must be trained individually, and it is not discussed how this can lead to a flexible reaching mechanism without suffering from catastrophic interference.

The model in [37] is used to obtain characteristics of M1 activity given the required muscle forces to produce a movement. It is an open-loop, locally-linear model, where all connections from M1 directly stimulate a linear motoneuron. Among other things, it showed that representations of kinematic parameters can appear when the viscoelastic properties of the muscles are taken into account, giving credence to the hypothesis that M1 directly activates muscle groups. Outside of its scope are neural implementation, learning, or the role of spinal cord.

[95] proposes a 2-level hierarchical controller for a 2-DOF arm. Since this model is based on optimal control theory, it is given a cost function, and proceeds by iteratively approaching a solution of the associated Jacobi-Bellman equation. There is no neural implementation of these computations, nor a description of learning.

[96] is not properly a neural model, but it is rooted in Dynamic Field Theory, which assumes that the population of neuronal activities encodes "activation variables". For this model activation variables represent kinematic parameters as a virtual joint location vector $\lambda(t)$, which is an internal representation of the arm's configuration.

The innovative part of [96] is in describing how $\lambda(t)$ is updated and used to control a redundant manipulator. In particular, the kinematic Jacobian, its null-space matrix, their derivatives, and the Moore-Penrose pseudoinverse are all computed analytically in order to obtain differential equations where the joint motions that move the end effector decouple from those which don't.

Encapsulating the muscle commands into a virtual joint location whose dynamics are decoupled for motions that don't affect the end-effector location is a very interesting concept. Still, this is far from a neural implementation, and learning is not considered.

The model in [97] studies the long-term development of infant reaching using a PD controller, and an actor-critic mechanism implementing a neural version of TD-learning [98]. The 2-dimensional PD controller receives two desired joint angles (interpreted as an equilibrium position), producing appropriate torques. Since it uses the Equilibrium Point (EP) Hypothesis [99], the reaching portion of this model is tantamount to associating states with equilibrium positions. This model thus performs at a higher level of analysis. Our model could operate at the same level if we added a reinforcement learning component to learn S_P values allowing the hand to *touch* a target whose distance is known. [97] does not consider separate neuronal populations (e.g. spinal cord, sensory cortex), propagation delays, or low-level learning.

The model in [100] shows how reinforcement learning can be applied to redundant actuators, such as biological arms. It is, however, not a neural model.

In [101], a neural network produces predictions of visual input in order to deal with temporal delays in a sensorimotor system. The network used for this study uses non-local learning, and adds or destroys nodes as required during its operation. It is thus not biologically-plausible.

[65] is a reaching model that also considers the spinal cord as a highly-configurable controller. Corticospinal inputs are assumed to be step commands, which means that motor cortex operates in an open-loop configuration. In order to produce reaching based on these constant commands, a biologically-implausible gradient descent mechanism is required, where the same reach is performed for various values of a synaptic weight, keeping the value that led to the best performance. Furthermore, the model learns to reach one target at a time, which would require learning anew when the new target is more than 45 degrees apart.

As mentioned in the main text, in the context of rotational dynamics, the

model in [42] was used to produce desired muscle forces using a recurrent neural network. This model uses the FORCE algorithm [102] to adjust the weights of a neural network with activity vector $\mathbf{r}(t)$ so it can produce experimentally observed muscle activity $\mathbf{m}(t)$. Oscillatory dynamics arise when the model is constrained to be simple.

Although very insightful, this model is limited by the fact that equations 2 and 3 represent an open-loop configuration, where only the M1 dynamics are considered. In essence, the model is doing a function approximation with the FORCE algorithm. The question of how the training data $\mathbf{m}(t)$ is produced is not addressed, nor is the role of spinal cord or sensory cortex (but see their Supplementary Figure 1).

Other than the aforementioned model in [65], we are unaware of spinal cord models addressing arm reaching. When these models are coupled with a musculoskeletal system, it is usually for the control of one degree of freedom using antagonistic neural populations. We mention some examples next.

The spinal cord model in [103] inspired much of the subsequent work, organizing the spinal circuit into six pairs of populations controlling two antagonistic muscle groups at one joint. With this model, the effect of Ia and Ib afferent input was studied in various neuronal populations.

[104] used a model similar to that in [103] in conjunction with a one DOF musculoskeletal model to study the effect of Ia afferents in the modulation of reflexes. [105] also adapted a similar model, and used it to inquire whether Parkinsonian rigidity arose from alterations in reciprocal inhibition mediated by reduced dopamine.

The model in [106] has several features not found in [103], including a heterogeneous motoneuron population, and a mechanism to generate electromyograms. This was used to study the generation of the H-reflex, and response properties of the motor neuron pool [107].

The model in [108] goes beyond models such as [103] by using populations of genetically-identified interneurons. This model is used to study rhythm generating abilities of the spinal circuit, as well as coordination between flexors and extensors [109, 110]. Knowledge regarding the role of genetically identified spinal interneurons in movement generation is still evolving [111, 112, e.g.].

This paper focuses on mammals, but the spinal cord of simpler organisms is better characterized [113, 114, e.g.], and may lead to the first realistic models producing ethological behavior.

6.2 Possible implementations of the learning rule

The learning rule in equation 9 is a Hebbian rule that also presents derivatives, heterosynaptic competition, and normalization (e.g. removing the mean) of its terms. None of these is new in a model claiming biological plausibility (e.g. [68, 115, 116, 117]). We nevertheless mention possible ways for derivatives and normalized terms to appear.

Formally, the time derivative of a function $f : \mathfrak{R} \rightarrow \mathfrak{R}$ evaluated at time t is the limit $\frac{f(t+\Delta t)-f(t)}{\Delta t}$ as $\Delta t \rightarrow 0$. If f represents the firing rate of a cell, a

measure of change roughly proportional to the derivative can come from $f(t) - f(t - \Delta t)$ for some small value Δt . The most obvious way that such a difference may arise is through feedforward inhibition (for the e_j signal), and feedback inhibition (for the c_i signal). Feedforward and feedback inhibition are common motifs in spinal circuits [75].

A somewhat different way to approach a time derivative is by using two low-pass filters with different time constants:

$$\frac{df}{dt} \approx f_{fast}(t) - f_{slow}(t),$$

where

$$\begin{aligned} \tau_1 \dot{f}_{fast}(t) &= f(t) - f_{fast}(t), \\ \tau_2 \dot{f}_{slow}(t) &= f(t) - f_{slow}(t), \\ \tau_2 &\gg \tau_1. \end{aligned}$$

These principles are illustrated in [118], where they are used to explain negative-derivative feedback.

Low-pass filtering can also arise in the biochemical cascades following synaptic depolarization. The most salient case is intracellular calcium concentration, which has been described as an indicator of firing rate with leaky integrator dynamics [119]. Although the physiology of spinal interneurons has not been characterized with sufficient detail to make specific hypotheses, it is clearly possible that feedback inhibition and low-pass filtering are enough to approximate a second-order derivative.

The e_j, c_i terms in our learning rule are mean-centered. The most straightforward way to subtract a mean is to have inhibitory units with converging inputs (e.g. receiving all the e_j signals) providing input to the c_i units. The Ib interneurons [75] are one possibility for mediating this. Another possibility is that the mean-subtraction happens at the single unit level when the input (e_j) and lateral (c_i) connections are located at different parts of the dendritic tree. In particular, a larger level of overall input activation $\langle \ddot{e} \rangle$ could produce a scarcity of postsynaptic resources flowing from the main branches of the dendritic tree into the individual dendritic spines, resulting in reduced plasticity.

6.3 Limitations of the model

A model as simple as ours will undoubtedly be wrong in many details. The main simplifying assumptions of our model are:

- **Firing rate encoding.** Each unit in this model captures the mean-field activity of a neuronal population. This may occlude computations depending on spike timing, as well as fine-grained computations at the neuronal and dendritic level.
- **Trivial sensory cortex.** We assumed that sensory cortex conveyed errors directly based on static gamma afferent activity. Sensory cortex may

instead build complex representations of afferent activity. It would be interesting to test how the requirement of controllability could guide learning of these representations.

- **No visual information.** Should a visual error be available, it could be treated by M in a similar way to somatosensory errors. If the visual error holds a monotonic relation with the afferent signals, then it should be possible to adjust the long-loop reflex in order to reduce it. When the relation between the visual error and the afferent signals is not monotonic (e.g. in some context the afferent signals correlate positively, and in other negatively), an alternative approach involving reinforcement learning can be pursued [11].
- **Very gross anatomical detail.** The detailed anatomical organization of cortex and spinal cord is not considered.
- **Errors must be monotonic.** Muscle activation may not monotonically reduce visual errors. Moreover, the haptic perception of contact is dependent on the environment, so it would not make an appropriate error signal.
- **No short-loop reflex connections.** Direct connections from muscle and skin afferents to the spinal cord are not included in our model. Plasticity in these connections is likely to be guided by supraspinal signals [26]. Therefore, the long-loop reflexes learned by our model could, combined with models of short-loop reflex learning [120, e.g.] could potentially provide faster autonomous control.
- **No cerebellum, basal ganglia, or premotor cortex.**

Each of these omissions is also a possible route for improving the model. We aim to grow a more sophisticated model, but each new component must integrate with the rest, improve functionality and agree with biological literature.

A final limitation concerns proofs of convergence. Many factors complicate them for this model: transmission delays, noise, synaptic learning, fully neural implementation, as well as complex muscle and afferent models. We tested our results for many initial conditions (section 10), but this of course is no guarantee.

50 years ago Marr’s model of the cerebellum became a stepping stone to further theoretical and experimental progress, despite all its shortcomings [121]. We aspire our model to be the next step towards a complete model of motor control.

7 The synergistic model

As described in section 2.3 of the main text, we can also use a spinal cord model where spinal interneurons stimulate two alpha motoneurons (also described in the Methods). For this version of the network we used a different parameter set

(see section 14). We tested this both with one-to-one connections between M and S_{PA} , and with connections where each M unit received a linear combination of S_{PA} activities. As in the main text, figures depict the network with this last connection scheme, unless otherwise noted.

Figure S1 shows how the network begins to reduce the error after roughly 200 seconds of training. Results are similar to those of figure 2 in the main text. As can be observed, the hand still moves towards the targets, but the trajectories are not straight lines, and show traits of cerebellar ataxia.

As in the main text, after a training phase consisting of 16 reaches, we set the targets for center-out reaching. Figure S2 is the analog of panels B and C of figure 3 in the main text. Panel A shows the case for one-to-one connections between S_{PA} and M .

Figure S3 shows the distance to the target and the hand velocity as a function of time for the reaches in panel B of figure S2. A trait that becomes evident is that the hand is constantly moving for most targets. After an initial approach, the hand oscillates around the target. Due to these oscillations the average distance between the hand and the target is about 4 centimeters.

The properties regarding directional tuning are also present in the synergistic configuration. This is shown in figure S4, where the preferred direction vectors are plotted for all the M units. A bootstrap test shows 9 units significantly tuned to direction ($p < 0.001$), but it can be seen that PD vectors have varying lengths. When predicting the PD vectors using the vectors of panel B (see main text and Methods), the coefficient of determination was about 0.93. Panel C shows the average muscle tension for each of the targets. It can be observed that muscle tension may not correlate with muscle activity in some cases.

As in the main text, we also plot the PD vectors for the two cases of connectivity in figure S5. In both the case of one-to-one connectivity (panel A), and in the case of mixed S_{PA} errors in M (panel B), the modified Rayleigh test (see Methods) no longer shows significant bimodality, although this bimodality arises if we only use the PD vectors that are longer than the average. In this case the main axis of the PD distribution is 67 degrees for panel A, and 70 degrees in panel B.

The final test we performed for the synergistic configuration was for rotational dynamics. Using the same procedure as in the main text, we obtained figure S6. For this figure the sampling time was 2 seconds. The rotations in panel A (one-to-one connectivity) are not so clear anymore, but to a large extent, counterclockwise movement is still observed. For the case of one-to-one connectivity (panel A), the first jPCA plane captured 35% of the variance. In the case of mixed S_{PA} inputs in M (panel B), the first jPCA plane captured 41% of the variance.

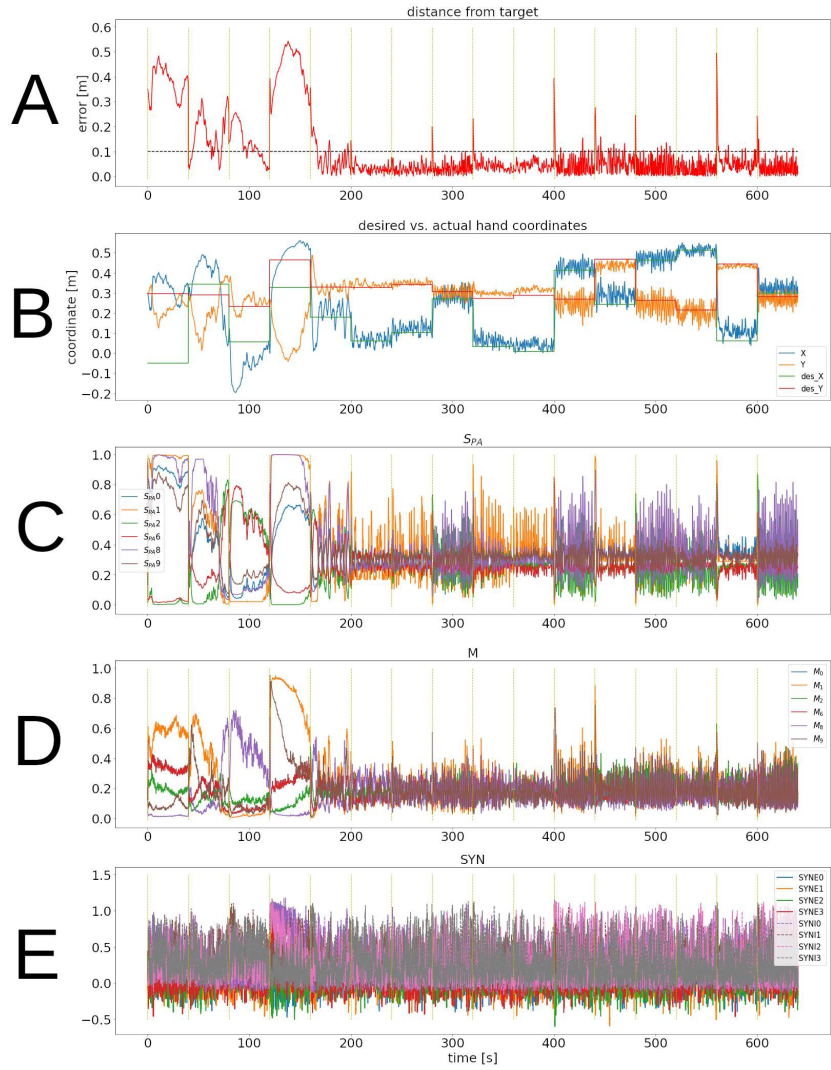


Figure S1: Training phase for the synergistic model. The errors errors in M are a linear combination of the S_{PA} errors. **A,B**: Captions as in figure 2 of the main text. **C**: Activity of 3 units in S_{PA} , and their duals. **D**: Activity of 3 units in M , and their duals. **E**: Activity of 4 excitatory spinal cord units (labeled "SYNEX"), and their corresponding inhibitory units (labeled "SYNLX").

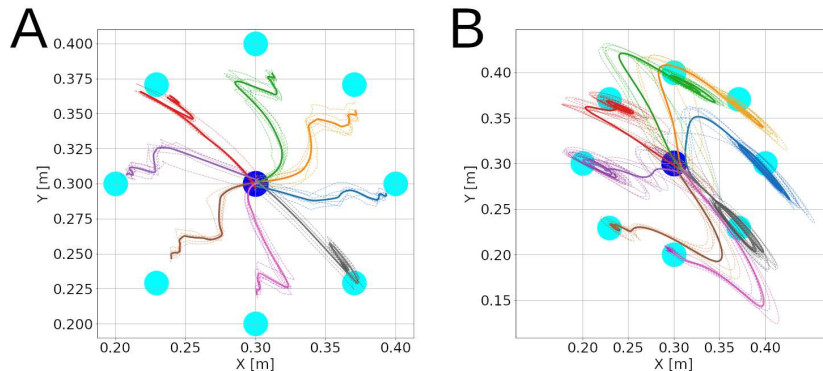


Figure S2: Hand trajectories for the center-out reaches. **A**: One-to-one connections between S_{PA} and M . Thick lines are the average of the 6 trajectories in thin dotted lines. **B**: “Mixed” S_{PA} errors in M .

8 Neural activity and synaptic weights during center-out reaching

Figure S7 shows the activity of some units during the 48 center-out reaches. This is analog to panels C,D,E of figure 2 in the main text. In addition we show how some of the synaptic weights evolve through time during these reaches.

During the center-out reaching phase a new target is being presented every 5 seconds, causing the spikes in activity appearing in all populations.

Panel D of figure S7 shows the value of the synaptic weights for all connections from M arriving in the first unit of the CE populations. Because of synaptic competition only a few weights can attain a large value, and it is observed that during the center-out reaching the weights are not in steady state. Jumps in the weight values are caused by jumps in the error every time the target changes. These jumps are probably harmful for the learning rule used in the connections from M to C , but they do not prevent the system from learning to reach.

Panel E shows a similar plot, this time for the weights of the connections from population A arriving on the first M unit.

9 Noise during center-out reaching

For the simulations in the main text, the noise in the CE , CI units was removed after the training phase was done. Decreasing the amount of exploration as time progresses is a common strategy in learning models. Nevertheless, it is pertinent to inquire whether center-out reaching can be done when noise is still present. The figures in this section illustrate traits of the reach trajectories when noise is not removed in the network of the main text.

Figure S8 shows the trajectories of the center-out reaches in the cases of

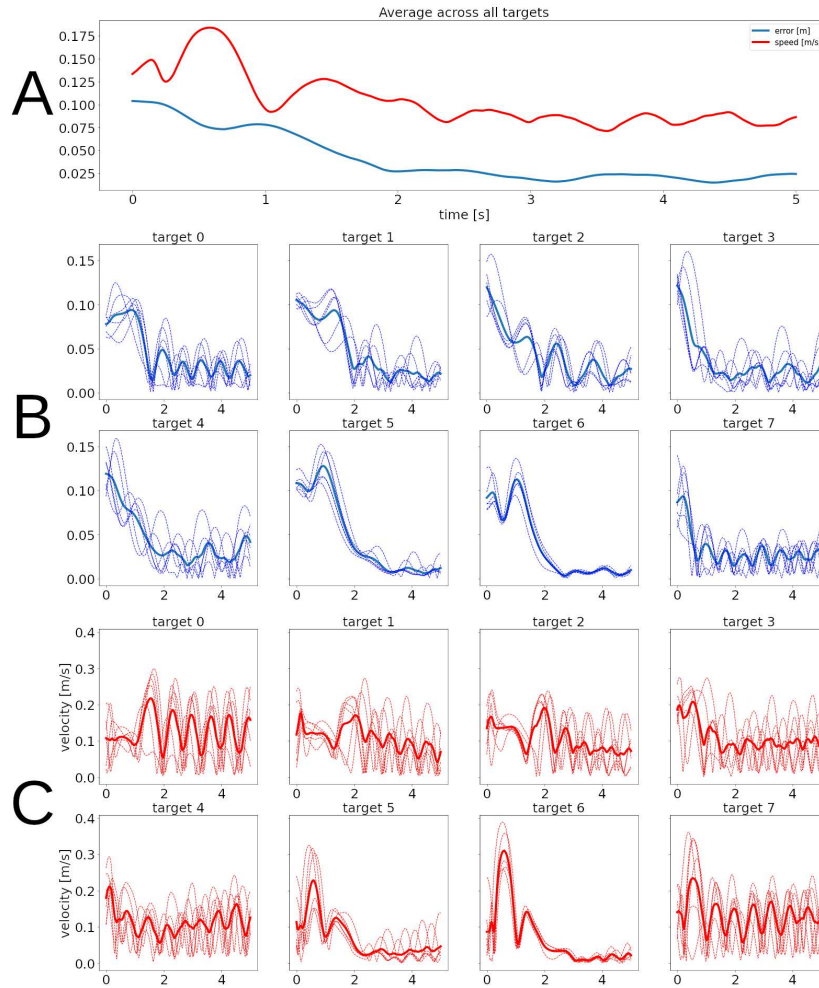


Figure S3: Distance to target and reach velocity for the synergistic configuration. **A:** Error and speed averaged across all targets as a function of time. **B:** Distance to target for individual targets, numbered as in panel A of figure 3. Thick traces show the average of the 6 individual trajectories, shown with dotted lines. **C:** Hand velocity for individual targets.

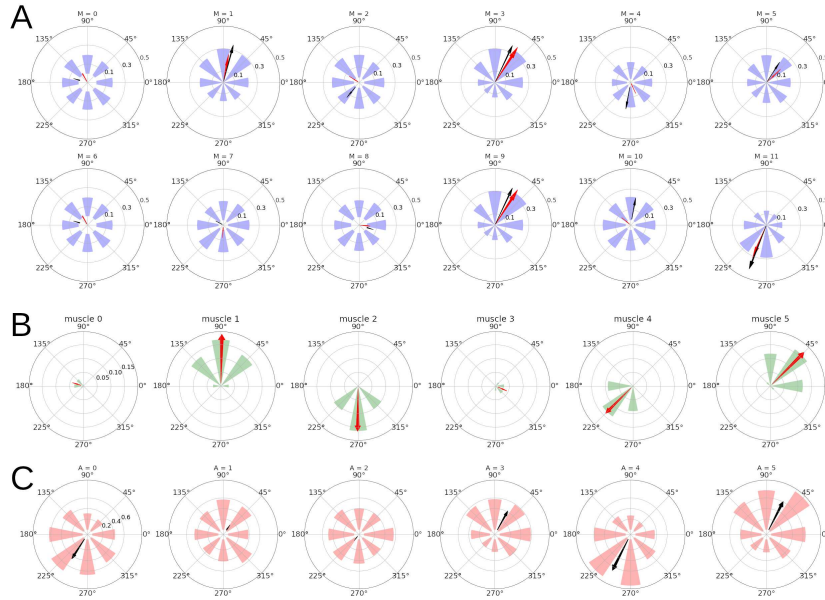


Figure S4: Directional tuning of the units in M using the synergistic configuration. Captions are as in figure 5 of the main text, but in this case the predicted PD vectors are not the same as the red arrows in panel B.

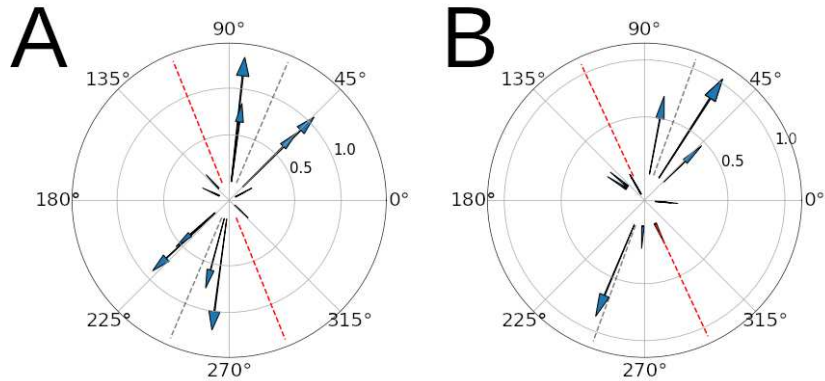


Figure S5: Distribution of PD vectors using the synergistic configuration. Captions as in figure 6 of the main text.

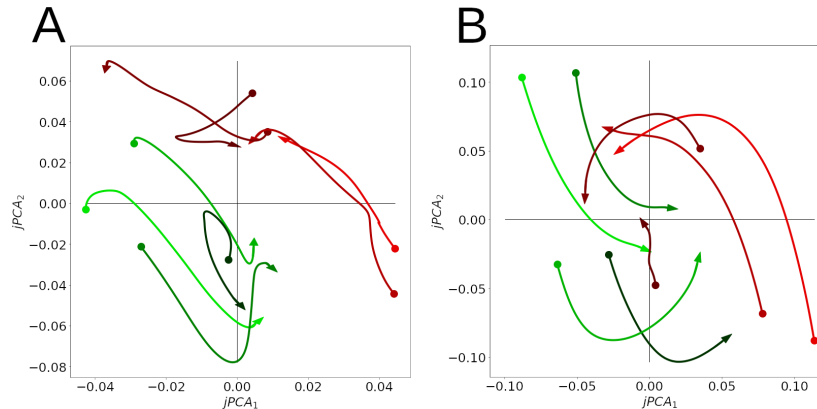


Figure S6: Rotational dynamics in the M population for the synergistic configuration. Captions are as in figure 7 of the main text.

one-to-one connectivity (panel A), and “mixed” S_{PA} errors in M . It can be seen that these are noisier versions of the trajectories in figure 3 in the main text. For the cases in both panels, the average distance between the hand and target is about 4.2 centimeters.

Figure S9 shows that the distance to the target is still reduced, but unlike figure 4 of the main text, velocity does not decrease significantly, and plenty of variation is seen in all reaches. This is also observed in figure S3.

Unlike figure 5 of the main text, figure S10 shows the case of the network with mixed S_{PA} inputs in M , with 10 units significantly tuned to reach direction (bootstrap, $p < 0.001$). The PD vectors can still be predicted from a linear combination of the vectors in panel B, with a coefficient of determination $R \approx .96$. Moreover, the PD vectors still align along a main axis, which can be observed in figure S11.

For both panels of figure S11 the main axis had an angle of roughly 60.5 degrees. In both cases the PD distribution showed significant bimodality (bootstrap with modified Rayleigh statistic, $p < 0.001$).

10 Variations in the configuration of the model

The main text of the paper describes several possible variations to the model: interneurons stimulating one or two alpha motoneurons, units in M receiving one or many S_{PA} inputs, noise during center-out reaching, and different amounts of mass for the arm. Furthermore, the model has a large number of metaparameters, and variations where one or more of them is changed are countless.

To provide a sense of how the model performs under these variations, we selected 16 configurations of the model, and in figure S12 we illustrate two measures of error for each of them.

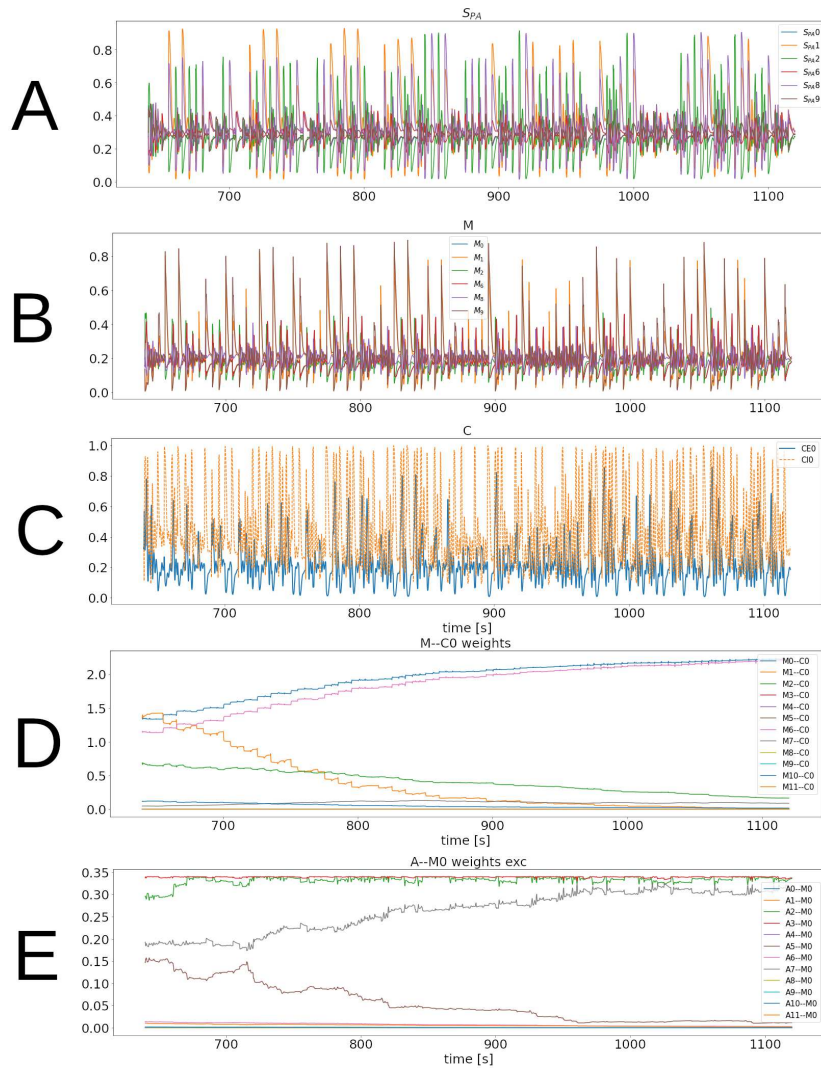


Figure S7: Unit activity and synaptic weights during center-out reaching. **A:** Activity of 3 S_{PA} units and their duals. **B:** Activity of 3 M units and their duals. **C:** Activity of 1 CE unit, and its corresponding CI unit. **D:** Synaptic weights of the 12 connections arriving on one CE unit from M . **E:** Synaptic weights of the 12 connections arriving on one M unit from A .

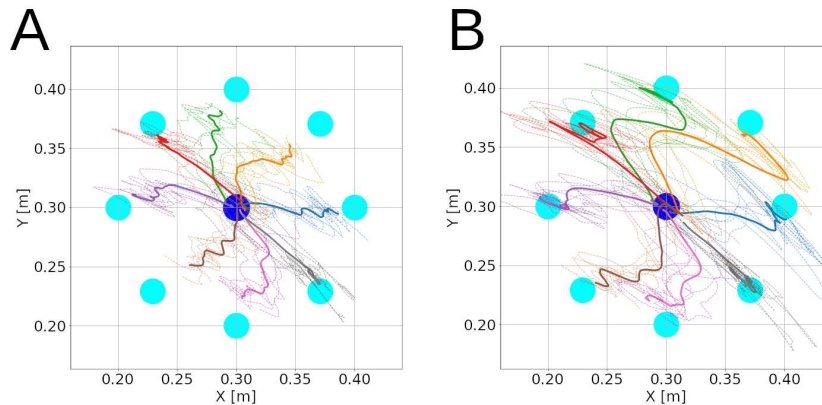


Figure S8: Hand trajectories for the center-out reaches with intrinsic noise in the CE, CI populations. Thick lines are the average of the 6 trajectories in thin dotted lines. **A:** One-to-one connections between S_{PA} and M . **B:** “Mixed” S_{PA} errors in M .

The 16 configurations of the model came after we selected 4 factors to explore: 1) parameter set, 2) gain level, 3) mixed S_{PA} inputs, and 4) synergistic configurations.

All the results in the main text use the same set of model parameters, which we will denote as “parameter set 1”. This was not our only candidate parameter set. All the results for supplemental section 7 use a different parameter set, “parameter set 2”. Which of these two sets to use is the first variation we consider.

The second variation, gain level, concerns how much the muscles are stimulated by a given level of motoneuron activation. To test this, after the training phase of the simulation we could increase the gain of the system by multiplying the input to the muscles times a 1.5 factor. The possibility of having this “high gain” configuration during center-out reaching constituted the second variation.

The third variation was whether M units received one-to-one or mixed inputs from S_{PA} units. The fourth variation was whether the synergistic configuration (e.g. spinal interneurons stimulating two alpha motoneurons) was used.

Possible combinations of these four binary variations yielded the 16 configurations. As for the error measures, we used the average distance between the hand and the target during two periods. The first period encompasses the last 4 reaches of the training phase (labeled “error_l4” in figure S12), and the second period consists of the center-out reaches (labeled “error_r”). For reference, the main text of the paper reports results with configurations 0 and 4 of panels A and B, whereas section 7 reports results from configurations 1 and 3 of panels C and D.

Since the particular value of these error measures may depend on the initial values of the synaptic weights, for each configuration we illustrate the mean and

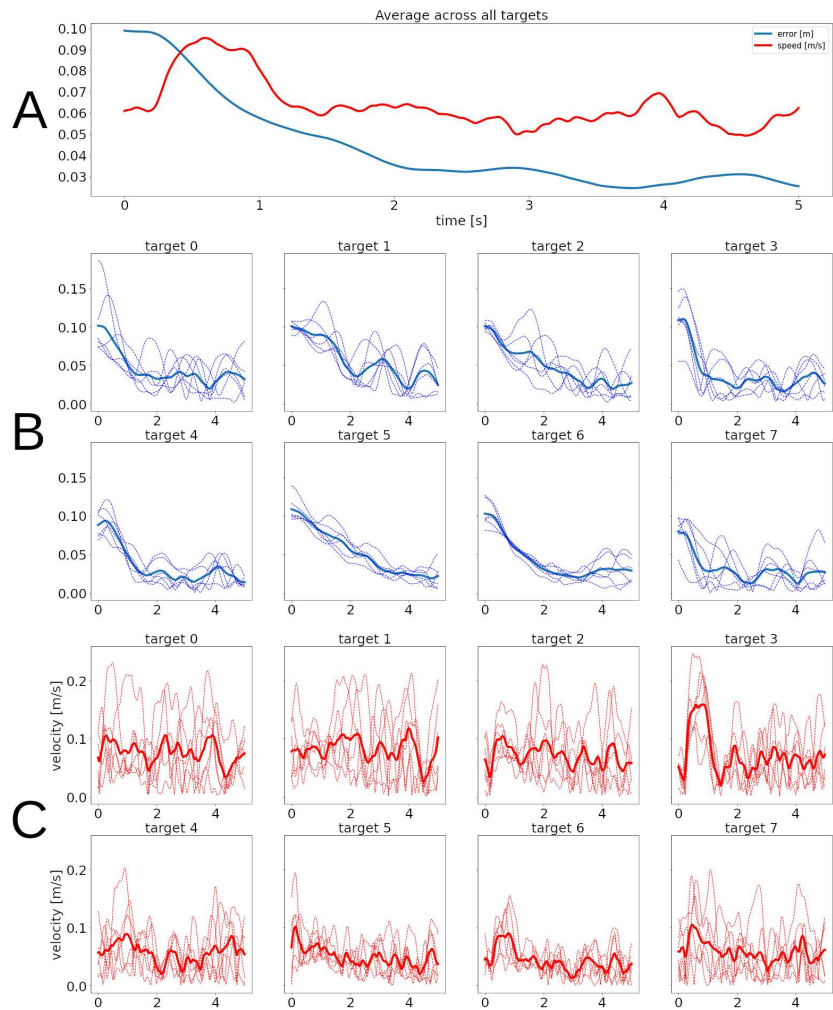


Figure S9: Distance to the target and hand velocity for all reaches using noisy C units. Captions are as in figure S3.

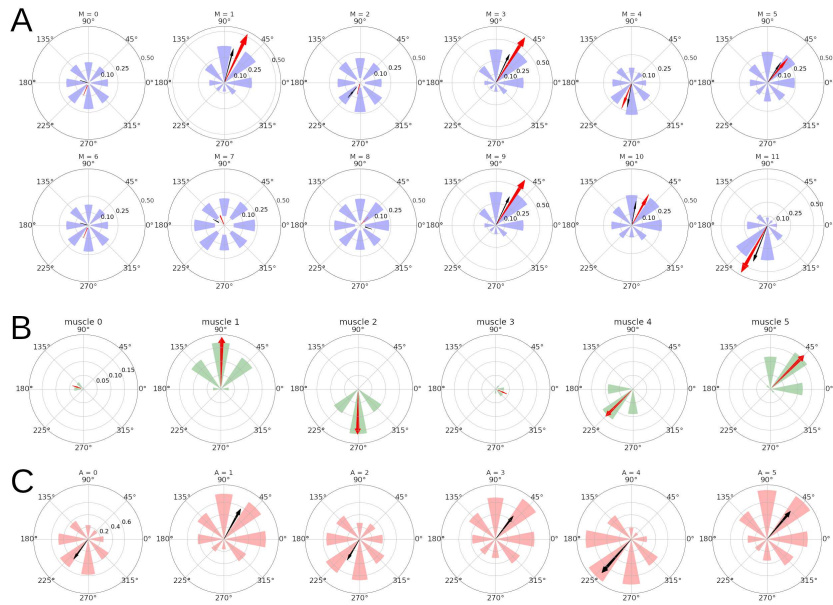


Figure S10: Direction tuning and PD vector for the M units when noise is present. Captions are as in figure S4.

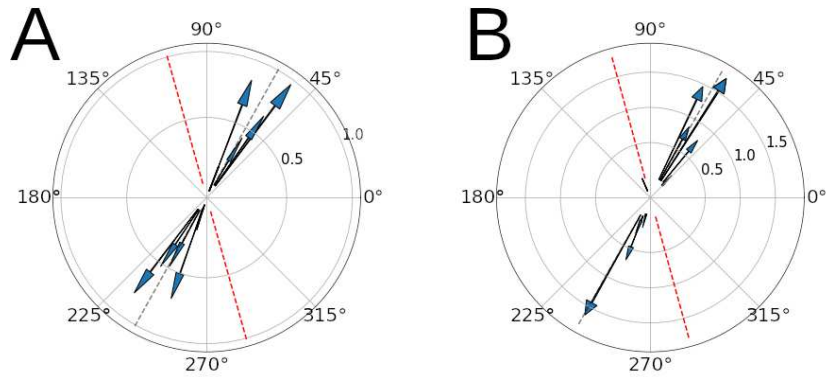


Figure S11: Preferred direction vectors for the 12 M units. Captions are as in figure 6 of the main text.

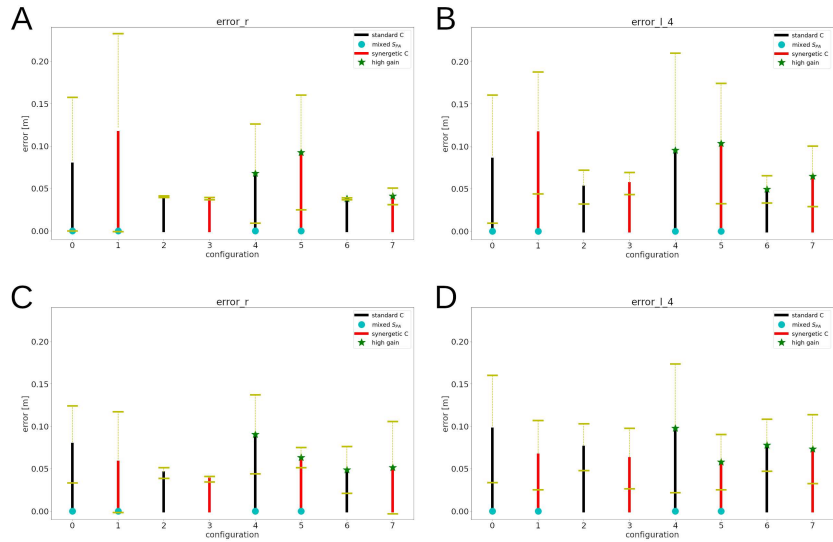


Figure S12: Error for different configurations of the model. The height of each bar represents the average error value for 20 simulations. Each of the 8 values in the horizontal axis corresponds to a different configuration. In each case, standard deviation is indicated by yellow horizontal lines. Black bars indicate that interneurons only activate a single motoneuron (labelled “standard C”); red bars indicate that interneurons activate two motoneurons (labelled “synergistic C”). Configurations with high gain are marked with a green star at the top of the bar. Configurations with mixed S_{PA} inputs to M are marked with a magenta circle at the bottom. **A:** Average error during center-out reaching when using the parameter set 1. **B:** Average error during the last 4 reaches of the training phase when using the parameter set 1. **C:** Average error during center-out reaching when using the parameter set 2. **D:** Average error during the last 4 reaches of the training phase when using the parameter set 2.

standard deviation from 20 separate simulations, each with a different seed for the random number generator. The results in all other sections of the paper use the same random seed, which was selected arbitrarily as the number 123456.

At first appearance figure S12 suggests that regardless of other factors, the most reliable configurations use one-to-one connectivity between M and S_{PA} . A closer look at the hand trajectories (e.g. figure S2), however, reveals that the situation is more subtle. In fact, configurations with mixed S_{PA} inputs generate larger muscle activation levels, in many cases leading the hand closer to the target than in the case with one-to-one connectivity. But this larger activation sometimes prevents the movement to cease once the error is small, leading to oscillations around the target. Or in some cases the hand may experience a large excursion before approaching the target.

Another aspect that deserves attention is that the error in configurations

0 and 1, both reported in the paper, has a large standard deviation, suggesting that some configurations still have a large error at the end of the training phase. Indeed 6 out of the 20 initial values had an “error_r” value larger than 5 cm for configuration 0, in parameter set 1, and the same number was found for configuration 1 in parameter set 2. Due to time limitations we have not determined whether longer training phases will reduce these errors, or whether the errors are due to the hand oscillating around the target (see supplementary videos 4,5,6 in section 13). Moreover, we have not implemented the strategy of starting learning with a large amount of exploratory movements which are gradually reduced in order to escape local optima.

11 The model fails when elements are removed

In this section we show the results of removing elements in the model. In particular, we show data for 3 cases: 1) There is no plasticity in the connections from M to CE and CI ; 2) there is no plasticity in the connections from A to M ; 3) the Ia, Ib afferents are removed, and information from the II afferents is sent to both M and S_F .

Figure S13 shows the error and hand coordinates though 16 training reaches for the 3 cases described above. As can be observed, the error is not permanently reduced, and the hand does not track the target.

Despite failing in the training phase, we still attempted center-out reaches for the 3 cases. The resulting hand trajectories can be observed in figure S14.

12 Results still hold when the arm changes its mass

The main text describes simulations where the mass of the arm and forearm are first reduced to 0.8 kg, and then increased to 1.2 kg. Figure S15 shows the hand trajectories for both of these cases.

As can be seen, reaching is not destroyed by the alterations in mass, and despite the sudden change from 0.8 to 1.2 kg, the mean trajectories still have a similar shape.

13 Supplementary videos

To help visualization of the arm’s learning and performance under different conditions, 7 videos were produced. To download these videos, please visit https://gitlab.com/sergio.verduzco/public_materials/, and navigate to the `adaptive_plasticity` folder. The videos are located in the `videos.tar.gz` file. In Linux and Mac systems they can be extracted with the command `tar xvfz videos.tar.gz`.

The videos’ content is described next.

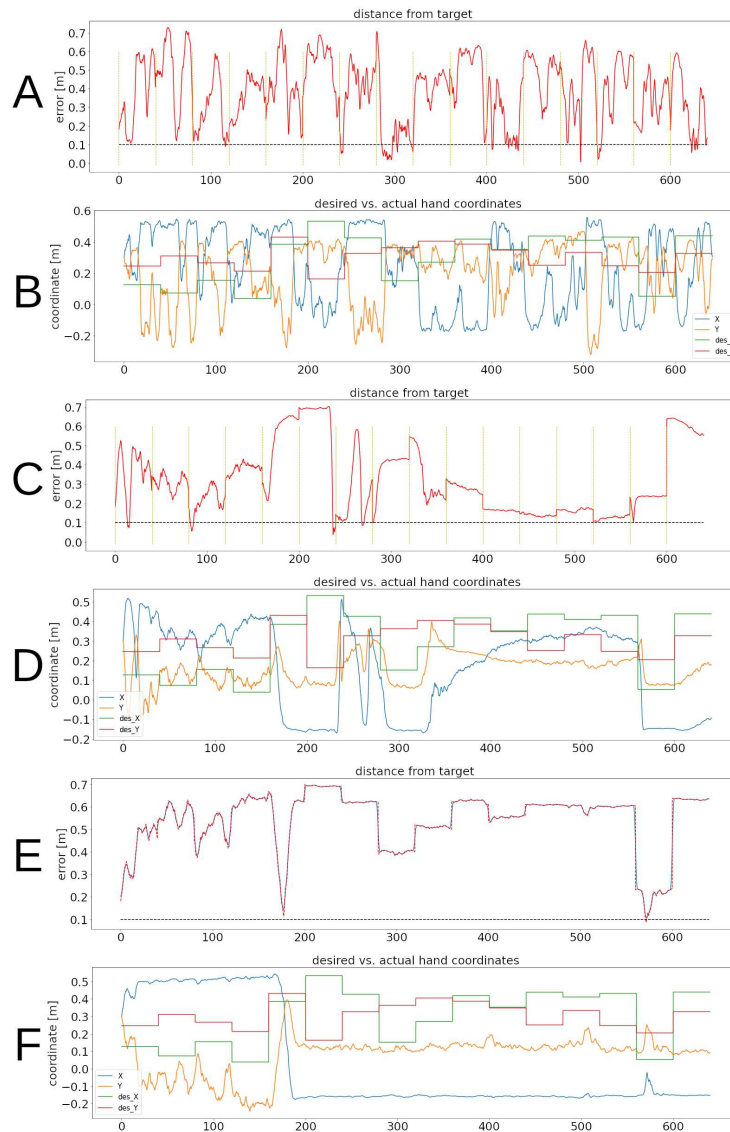


Figure S13: Distance from target, and hand coordinates when elements of the model are removed. **A:** Distance between hand and target when connections from M to C are static and random. **B:** Desired and actual X,Y hand coordinates for the case in panel A. **C:** Distance between hand and target when connections from A to M are static and random. **D:** Desired and actual X,Y hand coordinates for the case in panel C. **E:** Distance between hand and target when Ia and Ib afferents are removed. **F:** Desired and actual X,Y hand coordinates for the case in panel E.

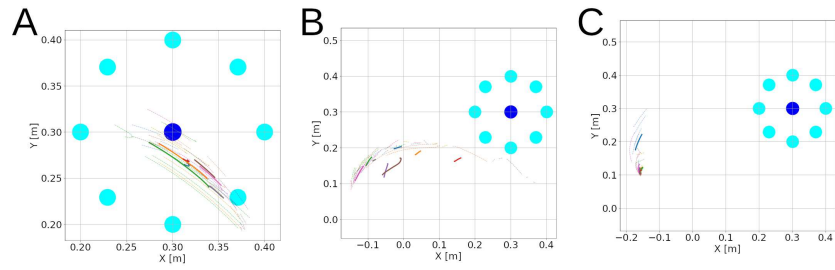


Figure S14: Hand trajectories when elements of the model are removed. **A:** Random static connections from M to C . **B:** Random static connections from A to M . **C:** No Ia or Ib afferents.

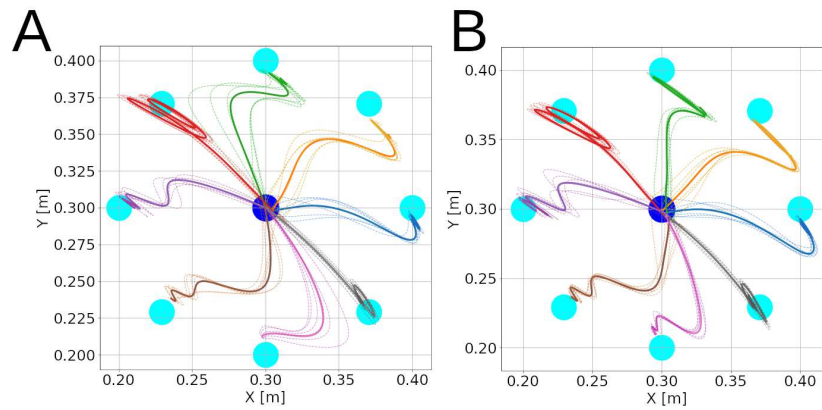


Figure S15: Hand trajectories with altered mass. **A:** Hand trajectories when both the arm and the forearm weigh 0.8 kg. **B:** Hand trajectories when the arm and the forearm weigh 1.2 kg.

- **SV1.mp4.** This video shows the arm during the first 640 seconds of the simulation, when the initial 16 training reaches are done. Referring to the variations in section 10, this network uses the first parameter set, mixed S_{PA} inputs in M , no synergies, and normal gains. This same configuration was used for figure 3C.
- **SV2.mp4.** The same simulation as in SV1.mp4, during center-out reaching.
- **SV3.mp4.** For this video we used the same configuration of figure 3B; namely: parameter set 1, no synergies, normal gains, and one-to-one S_{PA} inputs in M . This and all the following videos are for center-out reaching.
- **SV4.mp4, SV5.mp4, SV6.mp4.** SV4.mp4 shows the center-out reaches in a simulation where learning was incomplete after the training phase. Because of this, trajectories in SV4.mp4 are still evolving. To observe how trajectories changed, a second round (SV5.mp4), and a third round (SV6.mp4) of 48 center-out reaches were done. As can be observed, eventually the hand was able to approach all targets, but oscillations were constant, especially around the center target. The combination of slow convergence and oscillations can lead to the larger error measures observed in section 10. For this video we used parameter set 2, mixed S_{PA} inputs, a synergistic configuration, and normal gains. The mixed S_{PA} inputs and the synergistic configuration tend to produce larger gains in the system, and this, combined with delays is the likely cause of the oscillations.
- **SV7.mp4.** In this video we used parameter set 2, a synergistic configuration and one-to-one S_{PA} inputs. This abolishes the oscillations in videos 4,5,6, presumably due to lower gains. There is, however, target undershooting. The trade-off between undershooting and oscillations is a hard one to avoid for simple feedback control in the presence of delays.

14 Parameter values

Parameters marked with * belong to parameter set 1, and those with ** are in parameter set 2. Unmarked parameters are common to both parameter sets.

14.1 Unit parameters

The superscript x on a population name indicates that a parameter has heterogeneous values. This means that a random value was added to the parameter for each individual unit. This random value comes from a uniform distribution centered at zero, with a width equal to 1% of the reported parameter value.

Parameter	Equation	Population	Value
τ_u	5	<i>CHG</i>	10 [ms]
		α, S_A, S_{PA}^x	20 [ms]
		<i>CE</i>	240*, 220** [ms]
		<i>CI</i>	60*, 25** [ms]
		<i>M</i>	12*, 33** [ms]
β	6	α^x, ACT	2
		<i>CE</i>	2.25*, 2.26**
		<i>CI</i>	3.9*, 3.8**
		M^x	2.5
		S_A	4
		<i>CHG, S_{PA}^x</i>	9
η	6	α^x	.56*, .55**
		<i>CE</i>	1.14*, 1.05**
		<i>CI</i>	1.37*, 1.34**
		M^x, ACT	1
		S_A units 0,3	.59*, .55**
		S_A units 1,2,4,5	.4
		<i>CHG</i>	.25
		S_{PA}^x	.1
ς	7	<i>CE, CI</i>	.5*, .47**
τ_a	8	<i>A</i>	10 [ms]
T	8	<i>A</i>	.2
		<i>I_{b, II} afferents</i>	
		<i>A</i>	0
		<i>I_a afferents</i>	
τ_{slow}	12, 13	<i>CE, CI</i>	2
θ_{ACT}	15, 16	<i>ACT</i>	.31
τ_{ACT}	16	<i>ACT</i>	10 [ms]
γ	16	<i>ACT</i>	8
α	17	<i>CHG</i> (synapse)	20

14.2 Learning rules

Parameter	Equation	Value
Δt	9	170*, 150** [ms]
α	10	500
λ	10	.03
ω_{sa}	10	1.87*, 2**
ω_{sb}	10	3.28*, 3.4**
α_{IC}	11	20
ω_s	11	1
ω_{max}	11	.34*, .33**

14.3 Muscles and afferents

Parameter	Equation	Value
K_{SE}	18	20 [N/m]
K_{PE}	18	20 [N/m]
b	18	1*, 1.1** [N · s / m]
g	18 muscles 0-5	[60, 60, 60, 60, 66, 69]*, [61.4, 61.4, 61.4, 61.4, 67.5, 70.6]** [N]
K_{SE}^s	19,20,21	2 [N/m]
K_{PE}^s	19,20,21	2 [N/m]
b^s	19, 21	.5 [N · s / m]
K_{SE}^d	19,20,21	1 [N/m]
K_{PE}^d	19	.2 [N/m]
b^d	19	2 [N · s / m]
l_0^s	19	.7
l_0^d	19	.8
g_{I_a}	20 muscles 0-5	[7.5, 25, 25, 7.5, 25, 25] [m^{-1}]
$f_s^{I_a}$	20	0.1
g_{II}	21 muscles 0-5	[5.46, 8, 8, 5.46, 8, 8]*, [5.8, 8, 8, 5.8, 8, 8]** [m^{-1}]
f_s^{II}	21	0.5
g_{I_b}	22	1
T_0	22	10 [N]
τ_g	23	50 [ms]

14.4 Connection delays and weights

Connections considered "local" used a delay of 10 [ms], unless those those connections implied a not-modeled disynaptic inhibition. All other connections had a delay of 20 [ms].

Source	Target	Delay
<i>A</i>	<i>M, S_A</i>	20 [ms]
<i>ACT</i>	<i>CE, CI</i>	
α	muscle	
<i>M</i>	<i>CE, CI</i>	
<i>M</i>	<i>M</i>	
afferents	<i>A</i>	
<i>CHG, S_{PA}</i>	<i>ACT</i>	
<i>S_{PA}</i>	<i>M, S_{PA}</i>	
<i>CE, CI</i>	α	10 [ms]
<i>CE, CI</i>	<i>CE, CI</i>	
<i>CI</i>	<i>CE</i>	
<i>S_A, S_P</i>	<i>S_{PA}</i>	
<i>S_P</i>	<i>CHG</i>	

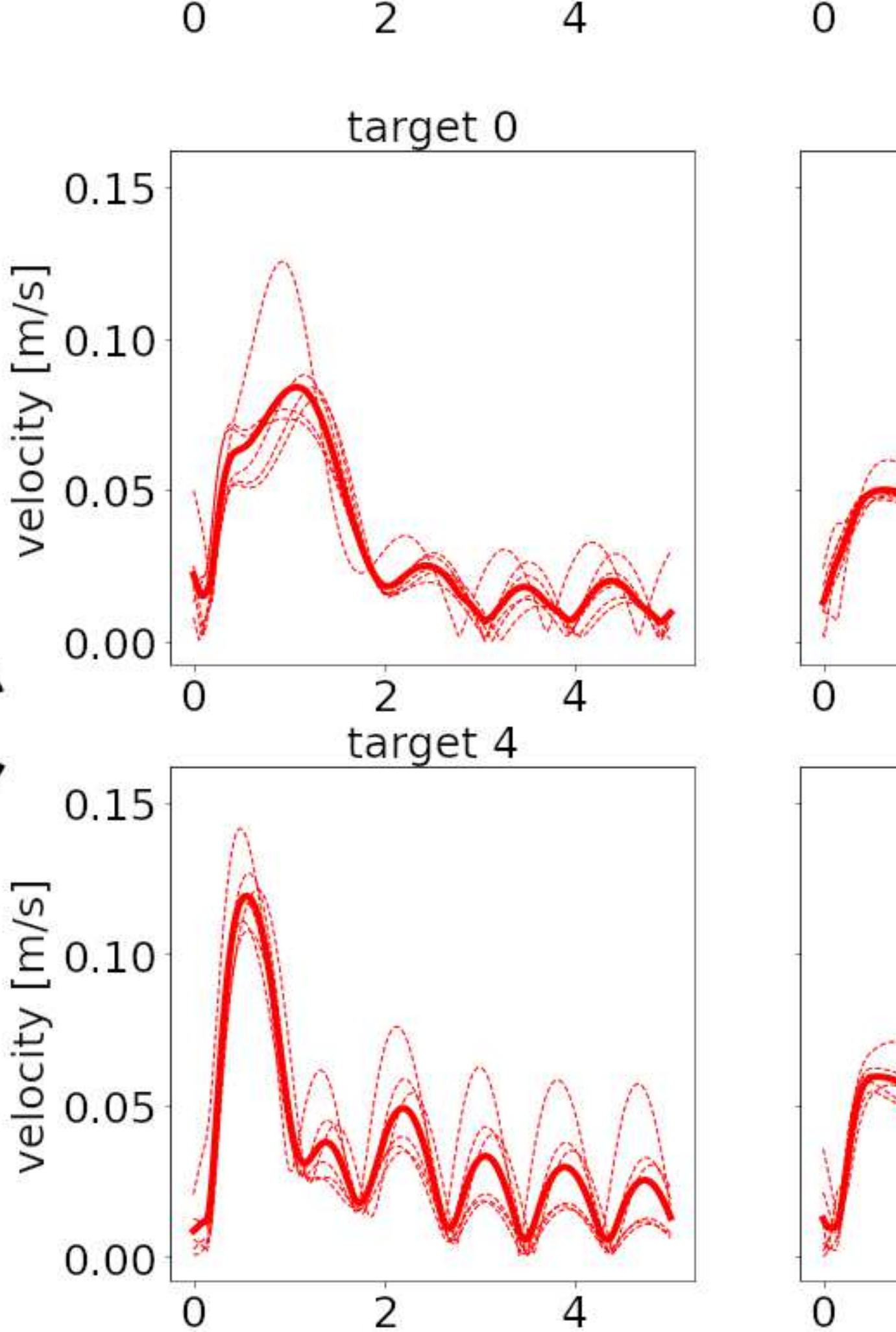
The next table shows the value of connections with fixed synaptic weights. Columns indicate the source of the connection, rows indicate the target. "Aff" stands for the muscle afferents. Plastic connections are marked as "+".

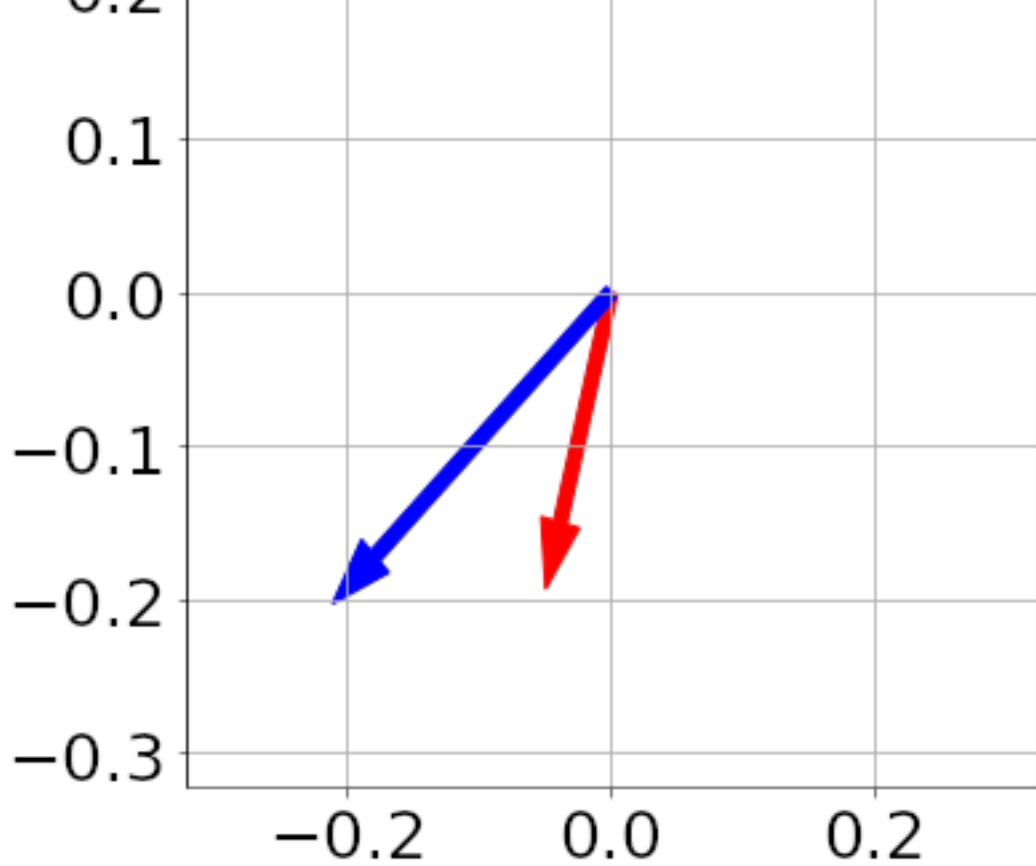
	α	<i>A</i>	<i>CE</i>	<i>CI</i>	<i>M</i>	Aff.	<i>S_A</i>	<i>S_P</i>	<i>S_{PA}</i>
α			1	-1					
<i>A</i>						2 (<i>I_a</i> , <i>I_b</i>), 4 (<i>II</i>)			
<i>ACT</i>									1
<i>CE</i>				-1.8*, -1.89**	+				
<i>CHG</i>								+	
<i>CI</i>			.39*, .38**		+				
<i>M</i>		+			0				*
muscle	1								
<i>S_A</i>		1							
<i>S_{PA}</i>							1 or -1	1 or -1	-1.6*, -1.77**

Connections between *CE, CI* populations in the table above are within the same (*CE, CI, α*) triplet. *CE* to *CE* connections use a weight of 1.1 in parameter set 1, and 1.13 in parameter set 2 for agonists. For partial agonists this becomes 0.26 for parameter set 1, and 0.33 for parameter set 2. *CE* to *CI* connections in antagonists use a weight of 1.6 in parameter set 1, and 1.7 in parameter set 2. For partial antagonists this becomes 0.15 in parameter set 1, and 0.27 in parameter set 2.

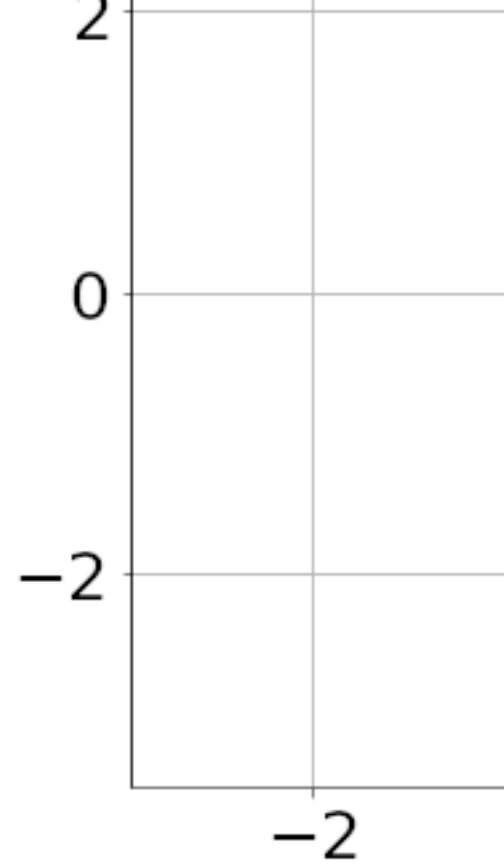
All connections whose source is *CHG* or *ACT* have a weight of 1. For the connections from *S_{PA}* to *M* see section 4.9 in the Methods.

C

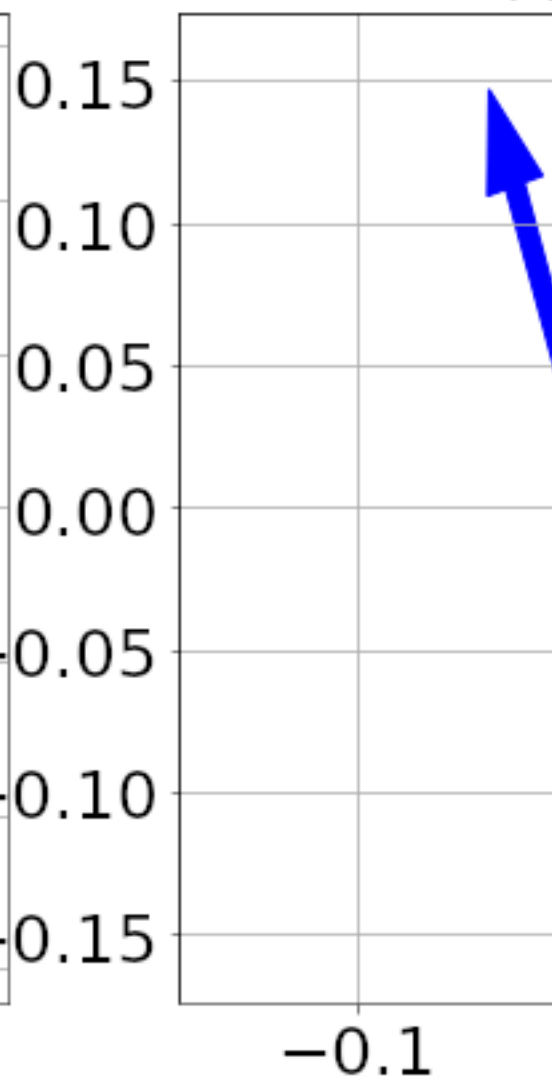
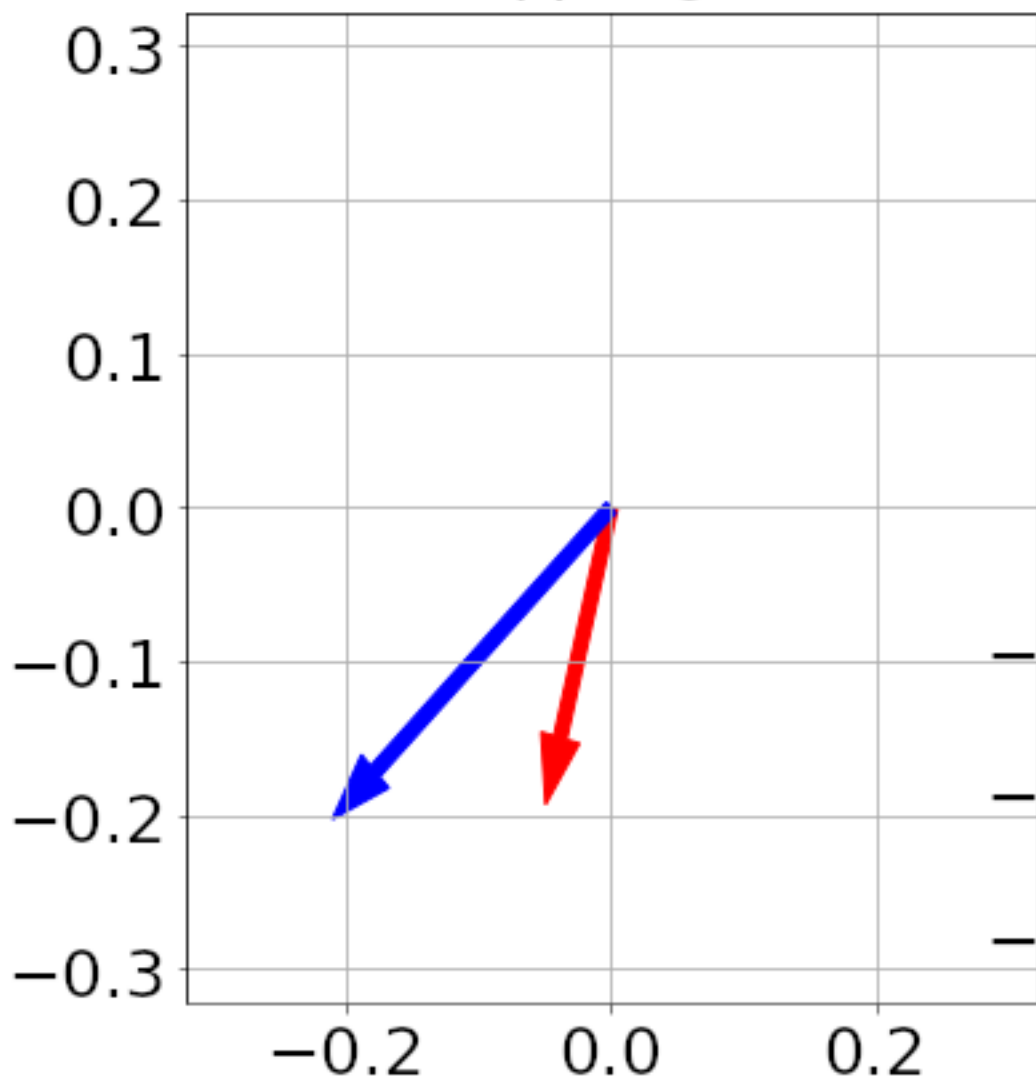


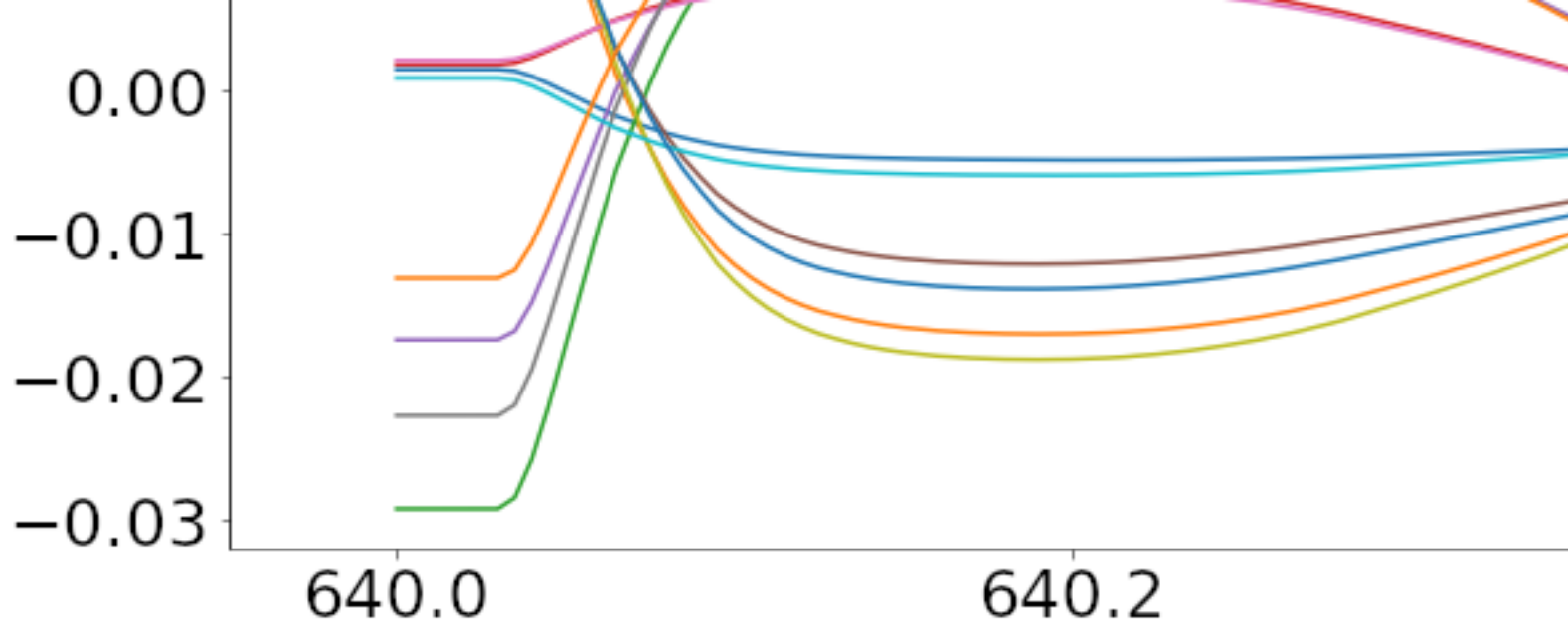


$M = 6$



M





C

